AD-A033 004 ROCKWELL INTERNATIONAL THOUSAND OAKS CALIF SCIENCE --ETC F/G 11/2
FAILURE PREDICTION IN CERAMICS USING ULTRASONICS.(U)
NOV 76 A G EVANS, B R TITTMANN, L A AHLBERG N00014-76-C-0624

UNCLASSIFIED SC5064.1TR NL

| OF |
AD
A033004

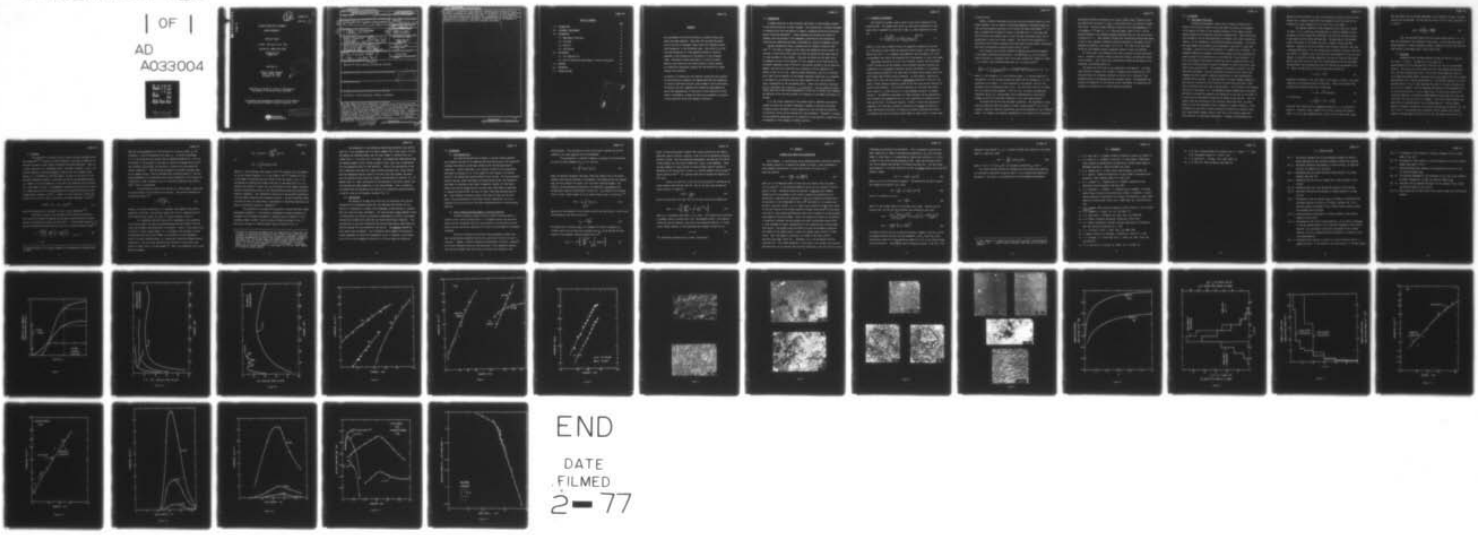

END

DATE
FILMED
2-77

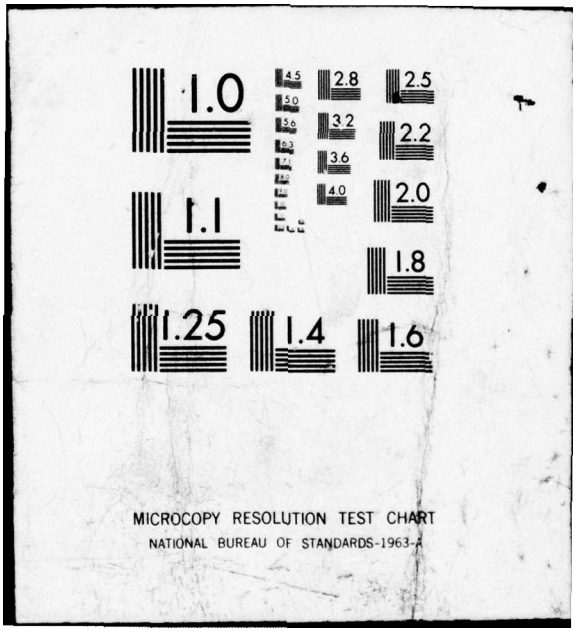
1.0
1.1
1.25
1.4
1.6
1.8
2.0
2.2
2.5
2.8
3.2
3.6
4.0
4.5
5.0
5.6
6.3
MICROCOPY RESOLUTION TEST CHART
NATIONAL BUREAU OF STANDARDS-1963-A

SC5064.1TR

COPY NO. 17

FAILURE PREDICTION IN CERAMICS USING ULTRASONICS

Technical Report

1st Mar. 1976 thru 31 Oct. 1976

Contract No. N00014-76-C-0624

Project No. 471
(NR039-129)

Submitted to:

Office of Naval Research
800 N. Quincy Street
Arlington, VA 22217

This Research was Sponsored by the Office of Naval Research
Under Contract No. N00014-76-C-0624 (Project No. 471)

Science Center
Rockwell International

Unclassified

SECURITY CLASSIFICATION OF THIS PAGE (When Data Entered)

REPORT DOCUMENTATION PAGE

READ INSTRUCTIONS BEFORE COMPLETING FORM

1. REPORT NUMBER

2. GOVT ACCESSION NO.

3. RECIPIENT'S CATALOG NUMBER

4. TITLE (and Subtitle)

(6) FAILURE PREDICTION IN CERAMICS USING ULTRASONICS.

5. TYPE OF REPORT & PERIOD COVERED
Technical
Mar. 1, 1976 thru Oct. 31,'76

6. PERFORMING ORG. REPORT NUMBER
(14) SC5064.1TR

7. AUTHOR(s)

(10) A. G. Evans, B. R. Tittmann, and L. A. Ahlberg

8. CONTRACT OR GRANT NUMBER(s)
(15) N0014-76-C-0624

9. PERFORMING ORGANIZATION NAME AND ADDRESS
Rockwell International
Science Center
Thousand Oaks, CA 91360
(11) 17 Nov 76

10. PROGRAM ELEMENT, PROJECT, TASK AREA & WORK UNIT NUMBERS
Project No. 471
(NR039-129)

11. CONTROLLING OFFICE NAME AND ADDRESS
Office of Naval Research
800 N. Quincy Street
Arlington, VA 22217 (Code 471)
(12) 46p.

12. REPORT DATE
Nov. 17, 1976

13. NUMBER OF PAGES
45

14. MONITORING AGENCY NAME & ADDRESS(if different from Controlling Office)
(9) Technical rept. 1 Mar - 31 Oct 76

15. SECURITY CLASS. (of this report)
Unclassified

15a. DECLASSIFICATION/DOWNGRADING SCHEDULE

16. DISTRIBUTION STATEMENT (of this Report)

Approved for Public Release; distribution unlimited

17. DISTRIBUTION STATEMENT (of the abstract entered in Block 20, if different from Report)

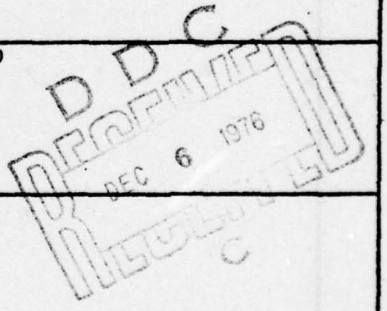

18. SUPPLEMENTARY NOTES

19. KEY WORDS (Continue on reverse side if necessary and identify by block number)

Ultrasonics, failure prediction, ceramics, attenuation

20. ABSTRACT (Continue on reverse side if necessary and identify by block number)

The requirements for failure prediction in ceramics using ultrasonics have been examined. These show that the absolute prediction of failure at acceptable stress levels and lifetimes requires high frequencies, in the 50-400 MHz range. The ability to utilize such high frequencies for flaw detection studies is primarily dependent on the attenuation of the material in this frequency range. Attenuation studies performed on a variety of ceramic materials have shown that the coarse grained or porous ceramics are excessively attenuating, whereas the fine grained fully dense ceramics are acceptable. → next page -- Continued

DD FORM 1 JAN 73 1473 EDITION OF 1 NOV 65 IS OBSOLETE

389949

Unclassified

SECURITY CLASSIFICATION OF THIS PAGE (When Data Entered)

An analysis of attenuation using numerical scattering cross sections and microstructural parameters has demonstrated that the attenuation is entirely predictable from the large extreme of the microstructure. The analysis has also suggested that attenuation measurements may permit the implementation of statistical failure prediction at high levels of confidence, in materials that are not amenable to absolute failure prediction using high frequency ultrasonics.

TABLE OF CONTENTS

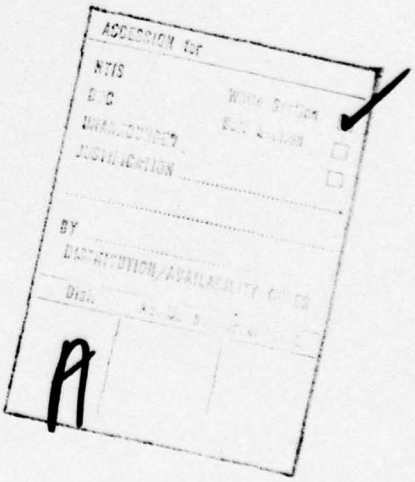

ABSTRACT

The requirements for failure prediction in ceramics using ultrasonics have been examined. These show that the absolute prediction of failure at acceptable stress levels and lifetimes requires high frequencies, in the 50-400 MHz range. The ability to utilize such high frequencies for flaw detection studies is primarily dependent on the attenuation of the material in this frequency range. Attenuation studies performed on a variety of ceramic materials have shown that the coarse grained or porous ceramics are excessively attenuating, whereas the fine grained fully dense ceramics are acceptable.

An analysis of attenuation using numerical scattering cross sections and microstructural parameters has demonstrated that the attenuation is entirely predictable from the large extreme of the microstructure. The analysis has also suggested that attenuation measurements may permit the implementation of statistical failure prediction at high levels of confidence, in materials that are not amenable to absolute failure prediction using high frequency ultrasonics.

1.0 INTRODUCTION

A primary restraint on the structural application of high strength ceramics is the large variability in their strength. The distribution in fracture strengths is related to the size distribution of defects introduced during the fabrication and/or finalizing operations.[1] A more extensive and reliable utilization of ceramics could be achieved if the components containing the most deleterious flaws could be identified and hence, eliminated as a source of premature failure.

The most deleterious flaws in ceramics are not uniquely related to their size.[1,2] The flaws in ceramics at the large size extreme are usually pores, inclusions or large grains (the latter are sites for machining flaws when they are in close proximity to the surface). Pores and inclusions are the major source of premature failure in fine grained ($\lesssim$ 10 μm) ceramics, while large grains are an equally important origin of failure in the coarser grained ($\gtrsim$ 30 μm) materials. However, the role of an inclusion as an initiator of failure depends on its nature, as well as its size. Some are highly deleterious, such as an inclusion with a small elastic modulus (E) and thermal expansion coefficient (α_0) compared to the matrix or an inclusion that can react chemically with its environs to cause a degradation of the surrounding matrix. Others are relatively innocuous, such as inclusions with a similar E, α_0 to the matrix. Failure prediction techniques that rely on the direct determination of the size of defects must therefore be cognizant of the failure heirarchy as it pertains to the defect and material of concern.

It is the initial objective of the present study to determine the material systems for which the ultrasonic technique is capable of obtaining sufficient information about the defect size and composition, that the absolute prediction of structural failure can be achieved with high confidence. Thereafter, alternate failure prediction techniques will be explored for those materials systems which are not amenable to high frequency ultrasonic analysis.

2.0 ULTRASONIC REQUIREMENTS

The fracture of ceramics usually occurs by the direct extension of pre-existing flaws. The largest sharp crack, a_m, that can be tolerated in a component that is expected to survive for a time, t_i, after inspection is given by[1];

$$a_m = \left(\frac{K_c}{\sigma_a Y}\right)^2 \left[\frac{2}{2 + K_c^{n-2} A t_i \sigma_a^2 Y^2 (n-2)}\right]^{2/(n-2)} \qquad (1)$$

where K_c is the stress intensity factor for mechanical extension of the flaw, σ_a is the tensile stress (often the principal tensile stress in the element containing the flaw), Y is a parameter that depends on the flaw shape, and A and n are parameters that define the susceptibility of the material to slow crack growth.

Approximate evaluation of a_m for four structural ceramics (two hot pressed silicon nitrides and two hot pressed silicon carbides) obtained, assuming that 10,000 hours is an acceptable inspection interval and 300 MPa is an acceptable stress-sustaining capability, has shown that all defects which produce flaws with radii larger than 10-100 μm must be detected. For most defects, equating the defect size to the flaw size affords a conservative prediction of failure;[1] and hence, a defect detection capability based on the flaw sizes derived from eqn (1) would be quite adequate. The principal exceptions are inclusions that either have a smaller E, α_o than the matrix, or have degraded the matrix by chemical reaction.[1] The detection requirement for these precursors can be substantially more stringent than suggested by eqn (1); and a capability for detecting flaws even smaller than ~ 10 μm may be required. Further, to avoid the rejection of components with relatively innocuous inclusions and to ensure the absence of highly debilitating inclusions, an effective ultrasonic technique must be able to establish the type of the defect being probed, at least within a limited range

of possibilities.

Present ultrasonic techniques, which only use the reflected intensity as the defect indicator, are not capable of providing unambiguous information about the flaw size and character and hence, do not satisfy the above requirements.[3,4] At best, a probabilistic estimate of failure is provided (Fig. 1), such that some deficient parts are accepted (type I errors) and some satisfactory parts are rejected (type II errors and 'false' signals). The final failure probability is prescribed to be the most acceptable value consistent with the economic constraints that result from excessive rejection due to type II errors.[4]

This situation can be greatly improved by adopting more pertinent measures of the defect scattering characteristics. The amplitude, A_R, of an ultrasonic signal received by a transducer after it has been scattered by a defect of radius, r, is related to the transmitted amplitude, A_T, of a plane wave by[5];

$$\frac{A_R}{A_T}\left[f,\theta,r\right] = \left[\frac{vr}{f(4\pi)^{3/2}R^2}\right]\left[S(f,r,\theta)\right]\left[\sqrt{G_T(f)\,G_R(f)}\right]\left[\exp[-2R\,\alpha(f)\,]\right] \quad (2)$$

where f is the frequency, θ is the scattering angle, v is the wave velocity in the material, R is the distance between the defect and the transducers, S is the scattering at the defect, α is the attenuation of the material, and G is the transducer gain (including bond loss, $\xi(f)$). The first term in eqn (2) is simply the loss caused by beam spreading. (This loss can, of course, be extensively reduced by the use of a focussed beam, but the determination of the relation between A_R and A_T for non-planar situations is not a well-posed problem.)

The second term derives from the defect scattering. The scattering of plane waves by defects has been the subject of several recent studies,[6,7] and in consequence, numerical scattering calculations can now be performed for any ellipsoidal defect. For example, the frequency dependencies of the scattering of longitudinal

plane waves have been calculated for two typical defect types,[2] spherical voids and spherical WC inclusions in Si_3N_4, at three defect radii of potential interest (Fig. 2a,b). The two principal features to note are the strong dependence of S on frequency ($\sim f^4$) when $kr < 1$ (k is the wave number, equal to $2\pi/\lambda$), and the marked difference in the detected frequency characteristics for the void and the inclusion at $kr > 1$. These features indicate that the maximum scattered amplitudes, as well as much important information about the character of the defect, can be obtained by operating in the range, $1/3 \lesssim kr \lesssim 3$. For flaws in the size range 10-100 μm, the frequency regime of greatest interest is thus 10 to 400 MHz.

The third term is the transducer gain, which includes all losses associated with the transfer of acoustic energy to electrical energy, including bond losses at the interface. These losses can be minimized by optimizing the design of the transducer, the bonding system, etc.

The fourth, and final term is the attenuation of the material. The attenuation normally increases with increase in frequency and microstructural size[8], and could thus be an important constraint on the utility of ultrasonic flaw characterization in the appropriate high frequency regime. The measurement and analysis of attenuation is thus the key initial requirement for determining the viability of ultrasonics as a failure prediction technique.

3.0 ATTENUATION

3.1 Measurement Techniques

Attenuation measurements require that allowances be made for the nature of the radiation pattern of the sound beam, the effect of the geometry of the sample, the effect of the boundary conditions of the sample, and the energy absorbed by the transducer from each succeeding echo. These difficulties were overcome at low and high frequencies by different, but closely related procedures. At low frequencies, the following procedure was adopted. (1) A buffer was used between the transducers and the specimen in the form of a water bath (1-25 MHz), a fused silica rod (25-120 MHz), or a sapphire rod (>120 MHz). This procedure removed the transducer from the data analysis and thus eliminated the need to account for any energy loss or echo distortion in the transducer. (2) An on-line computer (Data General Eclipse) was used in conjunction with a fast gate and an analog-to-digital converter (Biomation) to obtain the Fourier transforms of each received echo. This procedure was necessary, especially for the broad band transducers, since the attenuation was found to vary rapidly with frequency and thus required a separate determination at each (monochromatic) frequency within the band. (3) The amplitude of the same frequency component in each echo was corrected for the diffraction incurred during the echo's travel path to eliminate the losses due to beam spreading. (4) The effect of the boundary conditions of the sample, i.e., the impedance mismatch between buffer and sample, was taken into account by comparing the attenuation for the case of the buffer on on both sides of the sample with that of the buffer on one side only. This procedure allows the calculation of the reflection coefficient which, for these materials with low attenuation values, represents a sizeable correction. These procedures plus some care in sample preparation (parallelism of opposite faces, and a sample/buffer diameter several times that of the radiation beam) were found essential for meaningful measurements. Although the measurements were

tedious and time consuming, at least the corrections (3) and (4) could be incorporated into a computer program which was designed to give the value for the attenuation at each frequency for just a few initial data inputs.

The approach employed at high frequencies was to work with a pulsed rf signal ($\sim$ 0.1 s) which was long enough that it could be regarded a single frequency, but short enough that reflections from the front and back surfaces of the sample could be easily distinguished. The amplitude of the reflected signal from the end of the buffer rod, with no sample in place, was then measured. Assuming the end of the buffer to be a perfect reflector, this gave a reference amplitude, A, for the incident wave on the end of the rod, from which the effects of transducer loss, and diffraction and attenuation in the rod, were removed. An optically polished sample with two parallel faces was then pushed against the buffer rod with a gold foil placed between the rod and the sample. The amplitude of the reflected wave from the interface was now measured to be ΓA. Hence, the amplitude B of the wave entering the sample was

$$B = A(1 - |\Gamma|^2)^{\frac{1}{2}} \tag{3}$$

Assuming an attenuation α per unit length in the sample of length ℓ, the signal returning to the interface would be $B \exp(-2\alpha\ell)$. Hence, the resultant echo reaching the transducer should have an amplitude

$$C = B(1 - |\Gamma|^2)^{\frac{1}{2}} \exp(-2\alpha\ell) \tag{4}$$

It follows that

$$\alpha\ell = \frac{1}{2}\left[\ell n(1 - |\Gamma|^2) + \ell n \frac{A}{C}\right] \tag{5}$$

Since the first return gives an independent measure of Γ, it is possible to measure α. Typically, when a sapphire rod is used to contact the ceramic, there is a fairly good impedance match, so most of the incident power passes

into the ceramic and an accurate measurement is not difficult to make. An error analysis can be performed. We find that for errors $\delta(|r|^2)$, $\delta(A/C)$, the error in α, $\delta(\alpha)$, is;

$$\ell\delta(\alpha) = \frac{\delta(|r|^2)}{1 - |r|^2} + \frac{\delta(A/C)}{A/C} \qquad (6)$$

Thus, the technique should only give serious errors when $|r| \to 1$; i.e., when the reflection at the interface is very large. In this case the system is better employed in a more conventional manner to compare the first echo from the back surface of the sample with a triple transit echo.

3.2 Test Data

Attenuation data have been obtained for MgO, PZT and ZnS, Si_3N_4 and SiC (Figs. 3, 4 and 5). The MgO was a fully dense, hot pressed material with an equiaxed grain structure (Fig. 6a) and no noticeable porosity. The ZnS was also fully dense, but had a more complex microstructure (Fig. 6b) that contained many twins. The silicon nitride materials were two fully dense hot-pressed samples (prepared from α-Si_3N_4 powder with 2 and 5 percent MgO additives) and a reaction bonded material. The coarsest features in the hot-pressed materials (Fig. 7a) were equiaxed particles of silicides, carbides, etc. up to 10 μm in diameter, with the remainder consisting of fine elongated grains of silicon nitride up to ~ 5 μm in length (Fig. 7b); while the primary microstructural features in the reaction bonded materials were pores (Fig. 8a,c) and inclusions (Fig. 8b) up to 60 μm in diameter. The silicon carbide samples were made from a hot pressed material and a sintered material. The hot pressed material contained a proportion of relatively large equiaxed inclusions (Fig. 9a) and a fine (~ 4 μm) equiaxed grain structure (Fig. 9d); whereas the sintered material contained some fine porosity (Fig. 9b), and tabular grains (Fig. 9c).

3.3 Analysis

The scattering of ultrasonic waves by grains has been presumed by previous analysts[8,9,10] to derive from the difference in the elastic properties of the grain and matrix (small density differences have been neglected). Then, for a single large grain in a homogeneous matrix, the Lamé's constants, μ and λ, become the important scattering parameters; specifically, the scattering cross section, Ω, is determined by $(\Delta C)^2/C_o^2$, where C is equal to $\lambda+2\mu$ and ΔC is the difference between the modulus of the grain and that of the homogeneous matrix, C_o. However, since the attenuation is the sum of the scattering cross sections of a large number of grains, the fundamental scattering cross section of a grain in a random polycrystal can be characterized (for attenuation analysis) by the average elastic mismatch, $\langle (\Delta C)^2 \rangle$.* Further, for cubic materials, $\langle (\Delta C)^2 \rangle$ can be explicitly written in terms of the elastic stiffness constants, C, as;[8,10]

$$\langle (\Delta C)^2 \rangle = (C_{11} - C_{12} - 2C_{44})^2/75 \qquad (7)$$

Equivalent expressions are available for other crystal symmetries.[8,10]

The numerical value of the scattering cross section can be derived from the elastic mismatch by determining the power extracted from the incident wave by the scattered dilational and shear waves. In the Rayleigh regime ($kr < 1$), analytic expressions have been derived, and for an incident dilational wave;[8,10]

$$\Omega = \frac{4\pi^3 f^4 V_g^2}{5 v_\ell^4} \frac{(\Delta C)^2}{C_o^2} \left[1 + \frac{3}{2}\left(\frac{v_\ell}{v_s}\right)^5 \right] \qquad (kr \ll 1) \qquad (8)$$

$$\equiv \kappa V_g^2$$

---

*In textured materials, an average weighted by the predominant orientation must be used.

Note the strong dependencies of the scattering on the grain volume, V_g, the frequency, f, and the longitudinal wave speed, v_ℓ. At shorter wavelengths, $kr \approx 1$, the scattering cross section must be determined numerically. This can be achieved if the scatterer is described in terms of an average elastic stiffness constants, $\overline{C_{11}}$ and $\overline{C_{44}}$, and the matrix in terms of the polycrystalline elastic properties.[11] Then the energy scattered as dilational and shear waves can be computed using a recently developed exact scattering theory.[12] The frequency dependence of the scattering cross section determined in this fashion for large grains in MgO is plotted in Fig. 10, using the normalized cross section, $\Omega/2\pi r^2$, and kr as coordinates.

The scattering by pores can be derived in a similar manner, except that the elastic moduli of the scatterers are now zero. The analytic expression in the Rayleigh regime is[12]

$$\Omega = \frac{4\pi^3 f^4 V_p^2}{v_\ell^4} g_c \qquad (9)$$

where V_p is the pore volume and g_c is a parameter that depends on the elastic properties of the host, and typically ranges from 5 to 30. Computed values of the scattering cross section for pores in Si_3N_4 are plotted in Fig 10.

It is apparent from the strong size (V) dependence of the scattering cross section (eqns. 8,9) that the scattered energy derives primarily from the large size extreme of the distribution of scatterers. Hence, if the largest grain (or pore) in a small volume element, ΔV, is regarded as the scatterer, and the surrounding grains within that element are considered to be the homogeneous matrix, the total scattered energy, U_T, (neglecting interactions between adjacent scatterers) is the sum of the scattering cross sections of the extreme value grains (or pores) over all volume elements.[10] Hence, the attenuation (for a given material) becomes,

$$\alpha(f) \equiv \frac{1}{2} U_T(f) = \frac{1}{2} \sum_{i=1}^{i = 1/\overline{\Delta V}} \Omega_i(V_i, f) \qquad (10)$$

or,

$$\alpha(f) = \frac{1}{2} \int_0^\infty n(V_i)\Omega(V_i, f) dV_i$$

where Ω_i is the scattering cross section of the i^{th} scatterer, $\overline{\Delta V}$ is the median ΔV in unit volume of material, V_i is the volume of the i^{th} scatterer and $n(V_i)$ is the number of scatterers per unit volume in the size range V_i to $V_i + dV_i$. The problem of selecting the largest value from a fixed sample size, N, is an extreme value problem.[13] Hence, the size distribution of the largest scatterers should be characterized by one of only three possible extreme value distribution functions (Appendix). This substantial restriction of the possible distribution function greatly simplifies the attenuation analysis. The most convenient sample size would be that size below which a consideration of additional scatterers produces no significant increase in attenuation.*

The distribution of extreme value scatterers, derived from chord length measurements (Appendix), is conveniently represented for present purposes as a histogram, which indicates the number of scatterers per unit volume in a size (diameter) range D to D+ΔD. Grain size data for MgO are plotted in Fig. 11; while pore size data for reaction bonded Si_3N_4 are plotted in Fig. 12.

---

* The effect of increasing the sample size in a population of a fixed total size is simply to distort the distribution at small values of the variate; the distribution at large values of the variate is essentially unchanged. Therefore, properties determined by the large value extreme are not strongly dependent on the sample size. The minimum sample size should be that required for each large value scatterer to have a complete nearest neighbor array of matrix grains, i.e. 3 in a linear element or ~ 9 in a volume element. The optimum sample size for present purposes is in the range, ~ 5 to 10 for linear samples or ~ 30-200 for volume samples.

The attenuation is now obtained by taking the scattering cross section from Fig. 10 for the median grain (or pore) diameter ($\overline{D}$) in each range D to D+ΔD, and summing the scattered energy over the total number of scatterers per unit volume (Figs. 11, 12) within this size range. The attenuations predicted for MgO and reaction bonded silicon nitride, plotted in Figs. 13a,b, are in good accord with the attenuation data for both materials. Plots of the contribution to the total attenuation from each size range of grains and pores (Fig. 14a,b) confirm that the attenuation derives primarily from the large size extreme, and shows that the predicted values should be slightly underestimated (as observed, Fig. 13) because there is a small contribution to the attenuation from grains (pores) outside the measured range (especially at the large extreme). Also, as might be anticipated from the scattering cross section, the attenuation maximum displaces to smaller sizes as the frequency increases (Fig. 14).

3.4 Implications

The success of extreme value statistics and scattering cross section computations for attenuation prediction, has important implications for the analysis of attenuation in complex (multi-component) microstructures; a problem which has previously been intractable. The large extreme of each component within a microstructure can be easily evaluated by superimposing a grid on a micrograph and obtaining extreme value chord data for the pertinent phase (Appendix). The contributions to the total attenuation from each microstructural constituent can then be assessed from the scattering cross section. The dominant attenuating phase should then be apparent. This information would suggest microstructural design approaches for minimising attenuation, which, if feasible, would enhance the utility of high frequency ultrasonics as a failure prediction technique.

4.0 DISCUSSIONS

4.1 Flaw Detectability

The relative detectability of defects in various ceramic materials can be deduced from eqn (2) by combining the calculated values of the intensities scattered from defects and the bond scattering with the measured material attenuation. Typical amplitudes at the receiver (relative to the transmitted amplitude) are plotted in Fig. 15 for spherical voids located 1 cm from the surface in hot pressed and reaction bonded silicon nitride. For the hot pressed material the peak signal amplitudes are obtained above 50 MHz, and substantial amplitudes are retained to much higher frequencies; whereas, for the highly attenuating reaction bonded material the peak signal amplitudes are depressed to frequencies below 20 MHz, and very low signal amplitudes obtained above 40 MHz. High frequency ultrasonic analysis could thus be viable for the fully dense, fine grained materials that exhibit minimal attenuation; but is not expected to be of any value for the highly attenuating porous or coarse grained materials.

4.2 Role of Attenuation Measurements in Failure Prediction

Although ultrasonics cannot be used to identify discrete defects in materials with a coarse microstructure, it is suggested herein that the attenuation provides information about the large extreme of the microstructure that might allow the statistical prediction of failure to be performed with acceptable confidence.

Statistical methods have previously been unacceptable because they make the unwarranted assumption that the flaw population from batch to batch is invariant.[1] However, ultrasonic attenuation measurements on specific components, can provide information about the flaw population in that component, whenever the flaws are inherent flaws that relate to extreme value features of the

microstructure. This information can then be utilized to specify the failure probability for that component with high confidence.

The attenuation at a specific frequency is related to the distribution of grain (or pore) diameters, D_s, by (c.f. eqn 10)

$$2\alpha = \int_0^\infty n(D_s)\,\Omega(D_s)\,d\,D_s \tag{11}$$

Hence, by applying reasonable functional forms from n(D)dD (such as the second extreme value function described in the Appendix) and combining with the computed $\Omega(D_s)$ for the scatterer of concern, self consistent relations between α and $n(D_s)d\,D_s$ can be obtained by performing a few attenuation measurements over the pertinent range of microstructural variability. The probability of fracture P(S) of a small volume element ΔV_i at an applied stress level S is given by;[1,14]

$$P(S) = \Delta V_i \int_{D_{fc}(S)}^\infty n(D_f)\,d\,D_f \tag{12}$$

where D_f are the diameters of the fracture controlling flaws and D_{fc} is the critical flaw diameter, at the stress S, given by;

$$D_{fc} = 2\left(\frac{K_c}{SY}\right)^2 \tag{13}$$

The probability of fracture $D(S_m)$ of a component of volume V subjected to a variable stress S(x,y,z), which has a maximum value S_m, can be derived from the product of the elemental fracture probabilities as;[14]

$$P(S_m) = 1 - \exp\left[-\sum_{i=1}^{i=V/\Delta V_i} \Delta V_i \int_{Df_c(S)}^{0} n(D_f)d\,D_f\right] \tag{14}$$

Hence, if the microstructural elements that cause scattering are the same as those that control fracture, $n(D_f)dD_f$ in eqn (14) can be replaced by $n(D_s)dD_s$, derived as above from the attenuation measurements, and then eqn (14) can be solved uniquely for the fracture probability, $P(S_m)$, of the component. There are many examples of coarse grained or porous ceramics wherein fracture is dominated by the large grains or pores, e.g. reaction bonded silicon nitride,[15] coarse grained oxides.[16] This approach might thus be tenable for materials of this type.

Finally, we note that if the flaw size distribution is defined by the second extreme value function (eqn A5), then at the very large extreme that causes fracture it reduces to

$$n(D_f) = \frac{\beta}{D_f^{k+3}} \tag{15}$$

which on substitution into eqns (14) and (13) gives the failure probability;

$$P(S_m) = 1 - \exp\left[- \sum_{i=1}^{i - V/\Delta V} \Delta V_i \int_0^S \left(\frac{S}{S_o}\right)^{k+4} dS \right] \tag{16}$$

where S_o is a parameter containing k, β, K_c and V. This probability distribution is commonly found in strength tests (the 'two-parameter Wiebull' distribution), indicating that the exponent k that enters the attenuation behavior is related to the 'Wiebull modulus' m, that determines the strength variability, by;

$$m = k+4 \tag{17}$$

This interesting inference merits further investigation.

5.0 APPENDIX

EXTREME VALUE GRAIN SIZE DISTRIBUTIONS

Grain diameter, D, distributions can be obtained directly from planar sections. The simplest approach is to measure the lengths of chords, L, that correspond to grain boundary intersections at linear traces across the plane, and to apply the relation

$$n(D) = \frac{2n(L)}{\pi L^2} - \frac{2}{\pi L}\left[\frac{dn(L)}{dL}\right] \qquad (A1)$$

where n(L) is the measured number of chords per unit length in the size range L to L + dL and n(D) is the calculated number of grains per unit volume in the size range D to D+dD. Information about distributions in <u>specific</u> grain diameter regimes can also be estimated in this fashion, because the characteristics of grains within a specified size range derive from the corresponding characteristics of the chords in the neighborhood of that size.[18] Additionally, for extreme value analysis, since the fraction, ξ, of a linear trace occupied by extreme value chords is also the fraction of the volume occupied by extreme value grains,[18] a fixed sample size used for chord length determinations should also correspond to an approximately fixed number of grains per sample. Hence, the extreme value nature of the sampling is essentially retained, and the extreme value chord distributions should afford a close (although not exact) representation of the characteristics of the extreme value grains. The extreme value distribution can thus be estimated by measuring the lengths of the largest chords in equal size samples along a series of linear traces. Then, the number of chords per unit length of the trace, within a specified size range, yields n(L). Thereafter, n(D) can be obtained from n(L) using eqn (A1). This latter procedure is facilitated if the extreme value function describing n(L) can be obtained from the chord length data, such that eqn (A1) can be

transformed by performing the differential. This is achieved by plotting the chord length data in terms of the cumulative probability, $\Phi(L)$, that the chord length is larger than L (Φ is determined by simple order statistics, $\Phi \equiv i/n+1$), as shown in Fig. 16 for the data obtained on MgO. Then, the functional form of $\Phi(L)$ can be deduced from the best fit extreme value data plot. For most single phase materials, it has been found (Fig. 16) that the second extreme value function[13] pertains, namely;

$$\Phi(L) = 1 - \exp\left[-(L_o/L)^k\right] \tag{A2}$$

where L_o and k are distribution parameters. Differentiating eqn (A2) to obtain the frequency distribution, $\phi(L)$, gives

$$\phi(L) = \frac{k}{L^{k+1}} L_o^k \exp\left[-(L_o/L)^k\right] \tag{A3}$$

But n(L) is related to $\phi(L)$ by;

$$n(L) = \frac{\phi(L)\,\xi}{\bar{L}} \tag{A4}$$

where $\bar{L}$ is the average length of the extreme value chords. Substituting n(L) from eqn (A4) into eqn (A1) and performing the differential thus gives

$$n(D) = \frac{2k\,\xi\,L_o^{k-1}\exp[-(L_o/L)^k]}{\pi\,\Gamma(1-1/k)\,L^{k+3}}\left[2+k-k\left(\frac{L_o}{L}\right)^k\right] \equiv \frac{\beta\,\exp[-(L_o/L)^k]}{L^{k+3}}$$

$$n(D) \equiv \frac{2\,n(L)}{\pi\,L^2}\left[2+k-k\left(\frac{L_o}{L}\right)^k\right] \tag{A5}$$

The number of grains per unit volume with diameters between L and L+dL can thus be obtained directly from n(L) and the parameters k and L_o (the latter being derived from a best fit of the cumulative probability, $\Phi(L)$ to the second extreme value distribution). Finally, we note that by changing variables in eqn (A5), n(2a)

reduces at large values* ($L > L_o$) to another extreme value function of the second type (c.f. eqns (A3), (A4));

$$n(D) = \gamma \frac{\beta_o^{\alpha}}{\beta^{\alpha+1}} \exp[-(\beta_o/\beta)^{\alpha}] \qquad (A6)$$

where $\alpha = k/3$, $\beta = L^3$ and β_o and γ are constants containing L_o, k and ξ.

This result confirms the earlier statement that the extreme value sampling of the chords is equivalent (except at small L) to an extreme value sampling of the grains. This result is an essential part of the extreme value approach.

---

* In fact, because k is large (>5) for most grain and pore size distributions (see Fig. 16), L does not need to be much larger than L_o for eqn (A6) to pertain.

6.0 REFERENCES

1. A. G. Evans and T. G. Langdon, Progress in Materials Science, 21 (1976) 171.
2. A. G. Evans, B. R. Tittmann, G. Kino and P. T. Khuri-Yakub, 'Interdisciplinary Program for Quantitative Flaw Definition,' Science Center Report on ARPA/AFML Contract No. F33615-74-C-5180 (July 1976).
3. R. B. Thompson and A. G. Evans, Sonics and Ultrasonics, 23 (1976) 292.
4. D. P. Johnson, 'Inspection Uncertainty: The Key Element in Non-Destructive Inspection,' ERPI Technical Report 217-1 (May 1975).
5. B. R. Tittmann, D. O. Thompson and R. B. Thompson, Symposium on Non-Destructive Testing Standards, NBS (May 1976).
6. J. E. Gubernatis, E. Domony, J. A. Krumhansl and M. Huberman, 'The fundamental theory of elastic wave scattering by defects in materials - integral equation methods for application to ultrasonic flaw detection,' Report 2654, Materials Science Center, Cornell Univ. (ERDA Techn. Rpt. 100-3161-42) May 1976.
7. B. R. Tittmann, IEEE Ultrasonics Symposium (1976) Catalog No. 76 CH 1120-5SV (1976) 74.
8. E. M. Papadakis, J. Acoust. Soc. Am., 37 (1965) 711.
9. W. P. Mason and H. J. McSkimin, Jnl. Appl. Phys., 19 (1948) 940.
10. A. B. Bhatia, Ultrasonic Absorption (Oxford Univ. Press) 1967.
11. W. P. Mason, Piezoelectric Crystals and their Application to Ultrasonics, Bell Lab. Series (Van Nostrand, N.Y.) 1964.
12. C. S. Ying and R. Truell, J. Appl. Phys., 27 (1956) 1086.
13. E. Gumbel, Statistics of Extremes, (Columbia Univ. Press, N.Y.) 1956.
14. J. R. Matthews, F. A. McClintock and W. J. Shack, Jnl. Amer. Ceram. Soc., 59 (1976) 304.
15. A. G. Evans and R. W. Davidge, Jnl. Mater. Sci., 5 (1970) 314.

16. R. W. Rice, Fracture Mechanics of Ceramics (Ed. R. C. Bradt, F. F. Lange, D.P.H. Hasselman) Plenum, N.Y. (1974) p. 323.

17. J. W. Cahn and R. L. Fullman, Trans. AIME (1956) 610.

18. W. P. Reid, Jnl. Math and Physics, 34 (1955) 95.

7.0 FIGURE CAPTIONS

Fig. 1. The relation between flaw size and detection probability based on signal amplitude for two ultrasonic systems or sensitivity settings.

Fig. 2. Calculated scattering from defects in silicon nitride, (a) spherical cavities, (b) spherical WC inclusions.

Fig. 3. Attenuation data for three relatively coarse grained, fully dense ceramics, MgO, ZnS, PZT.

Fig. 4. Attenuation data for two hot pressed and a reaction bonded silicon nitride.

Fig. 5. Attenuation data for a hot pressed and sintered silicon carbide.

Fig. 6. Reflected light optical micrographs of etched surfaces of (a) MgO, (b) ZnS.

Fig. 7. Micrographs of the hot pressed Si_3N_4 with 5% MgO, (a) reflected light micrograph showing inclusions of silicodes, carbides, etc., (b) a scanning electron micrograph of an HF etched fracture surface showing the elongated grain structure.

Fig. 8. Scanning electron micrographs of fracture surfaces of the reaction bonded silicon nitride.

Fig. 9. Micrographs of the silicon carbide materials, (a) an optical micrograph of the hot pressed material, (b) an optical micrograph of the sintered material, (c) a polarised light optical micrograph of the sintered material, and (d) a scanning electron micrograph of a thermally etched hot pressed material.

Fig. 10. Scattering cross sections for pores in silicon nitride and grains in magnesium oxide; r is the radius of the scatterer and k is the wave number.

Fig. 11. A histogram of chord lengths (L) and grain diameters (D) for the MgO shown in Fig. 6(a).

Fig. 12. A histogram of chord lengths (L) and pore diameters (D) for the reaction bonded Si_3N_4 shown in Fig. 8.

Fig. 13. Predicted attenuations compared with the measured values for (a) MgO (b) reaction bonded Si_3N_4.

Fig. 14. The predicted dependence of the attenuation on the size of the scatterer at several frequencies, (a) MgO, (b) reaction bonded Si_3N_4.

Fig. 15. Predicted relative detected amplitudes for hot pressed silicon carbide and reaction bonded silicon nitride.

Fig. 16. Chord length data for MgO fitted to the second extreme value distribution function.

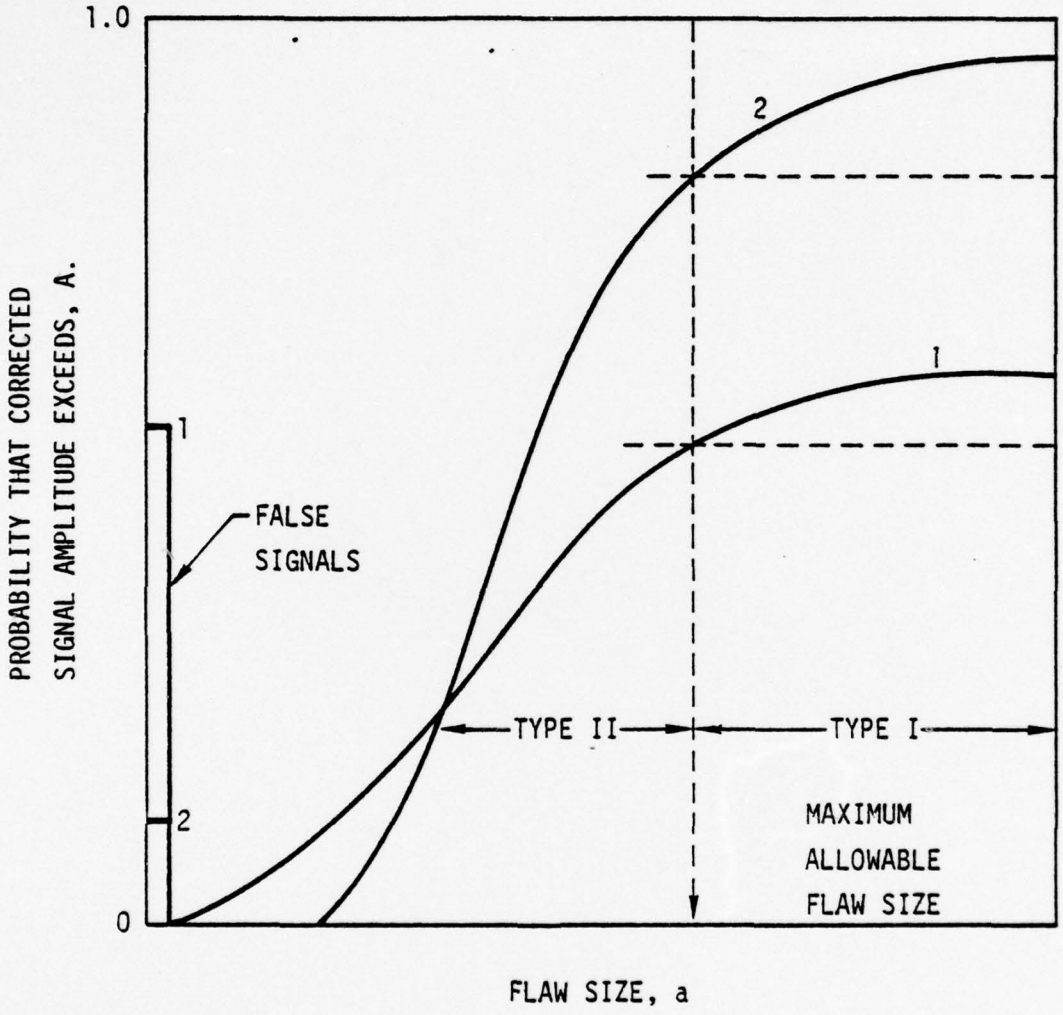
1.0
PROBABILITY THAT CORRECTED
SIGNAL AMPLITUDE EXCEEDS, A.
2
1
1
FALSE
SIGNALS
TYPE II
TYPE I
2
MAXIMUM
ALLOWABLE
FLAW SIZE
0
FLAW SIZE, a

Figure 1

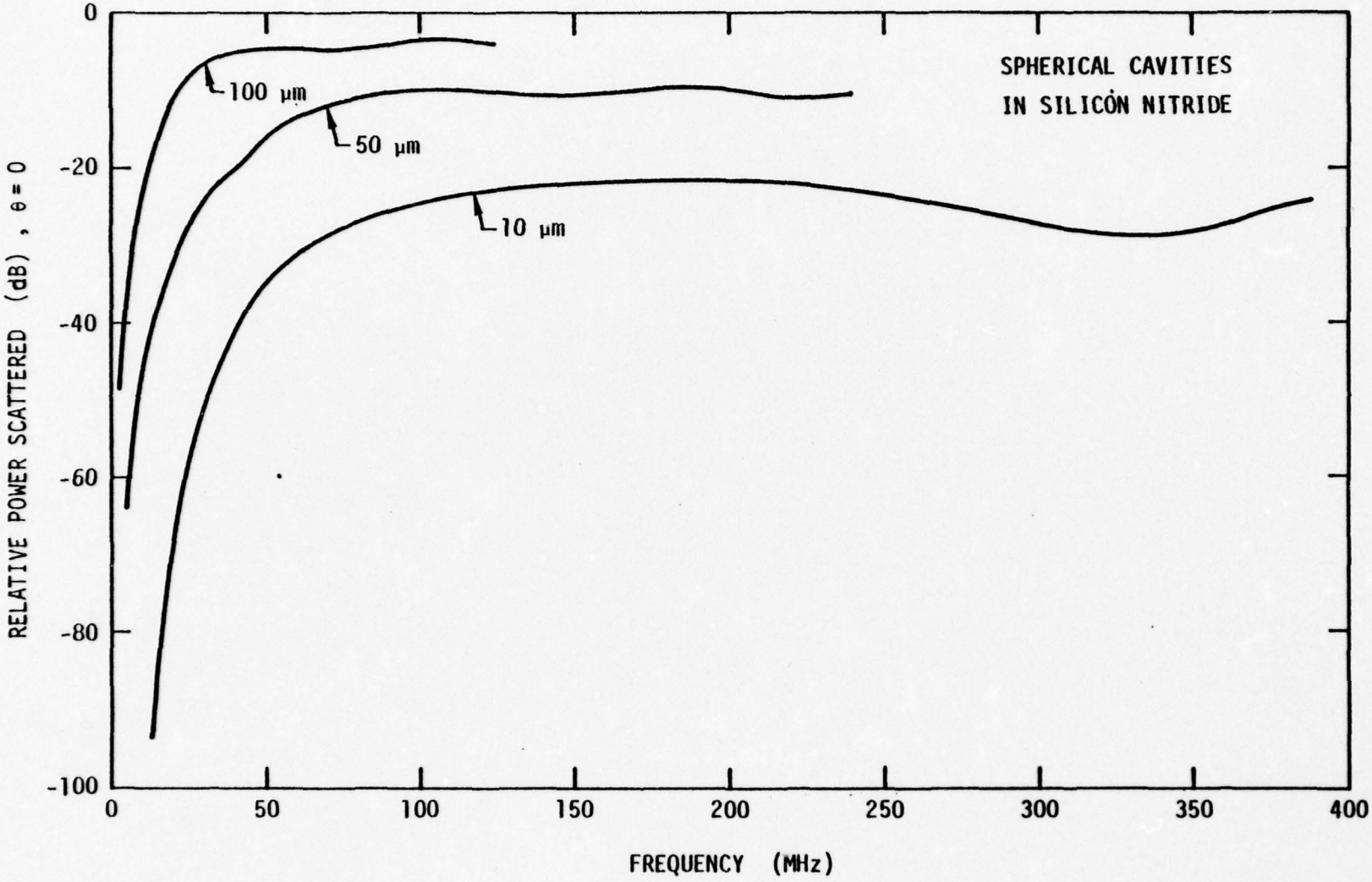
SPHERICAL CAVITIES
IN SILICON NITRIDE
100 μm
50 μm
10 μm
RELATIVE POWER SCATTERED (dB) , θ = 0
0
-20
-40
-60
-80
-100
0
50
100
150
200
250
300
350
400
FREQUENCY (MHz)

Figure 2 0

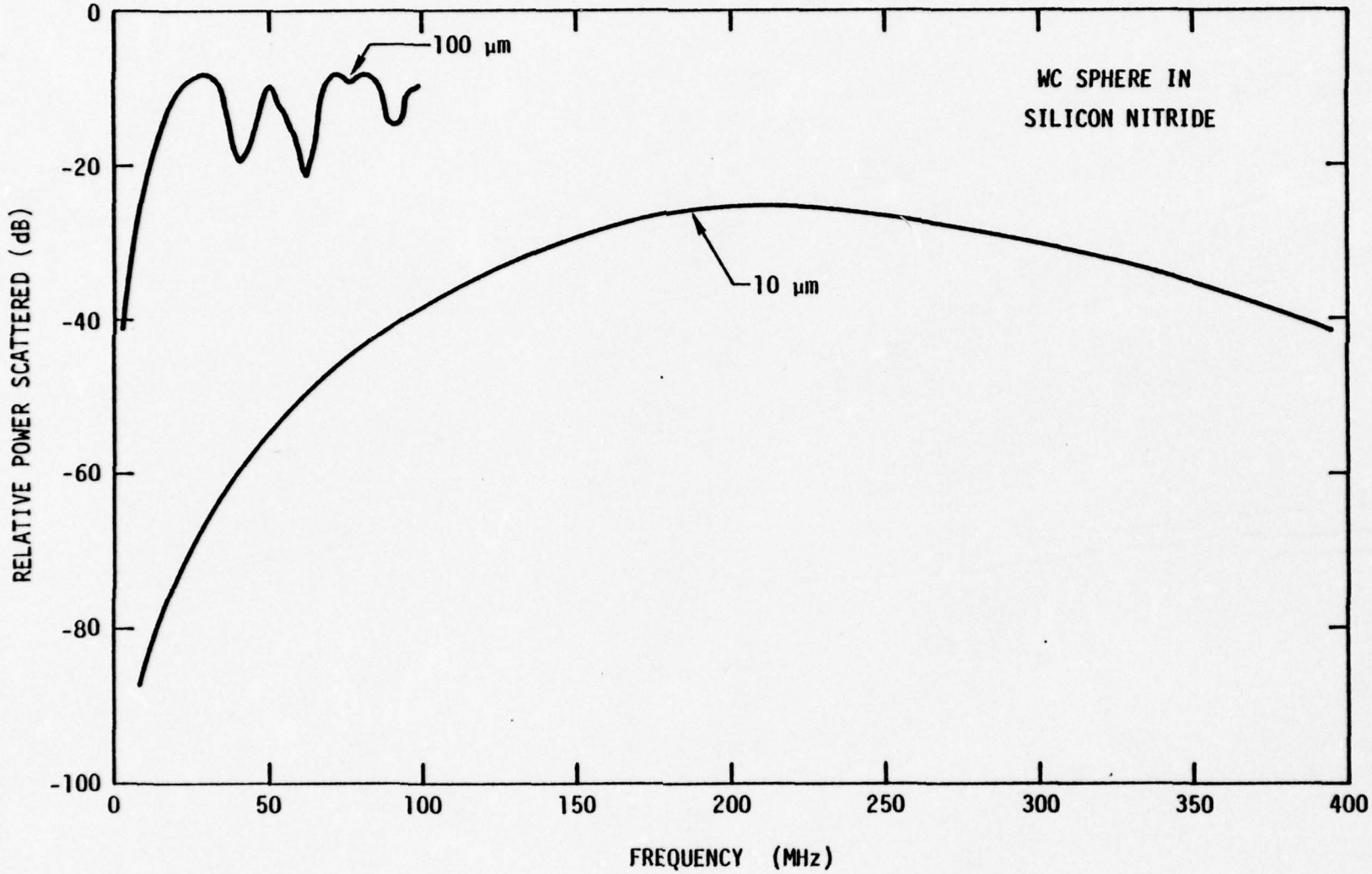
0
-20
-40
-60
-80
-100
0
50
100
150
200
250
300
350
400
100 μm
10 μm
WC SPHERE IN
SILICON NITRIDE
RELATIVE POWER SCATTERED (dB)
FREQUENCY (MHz)

Figure 2b

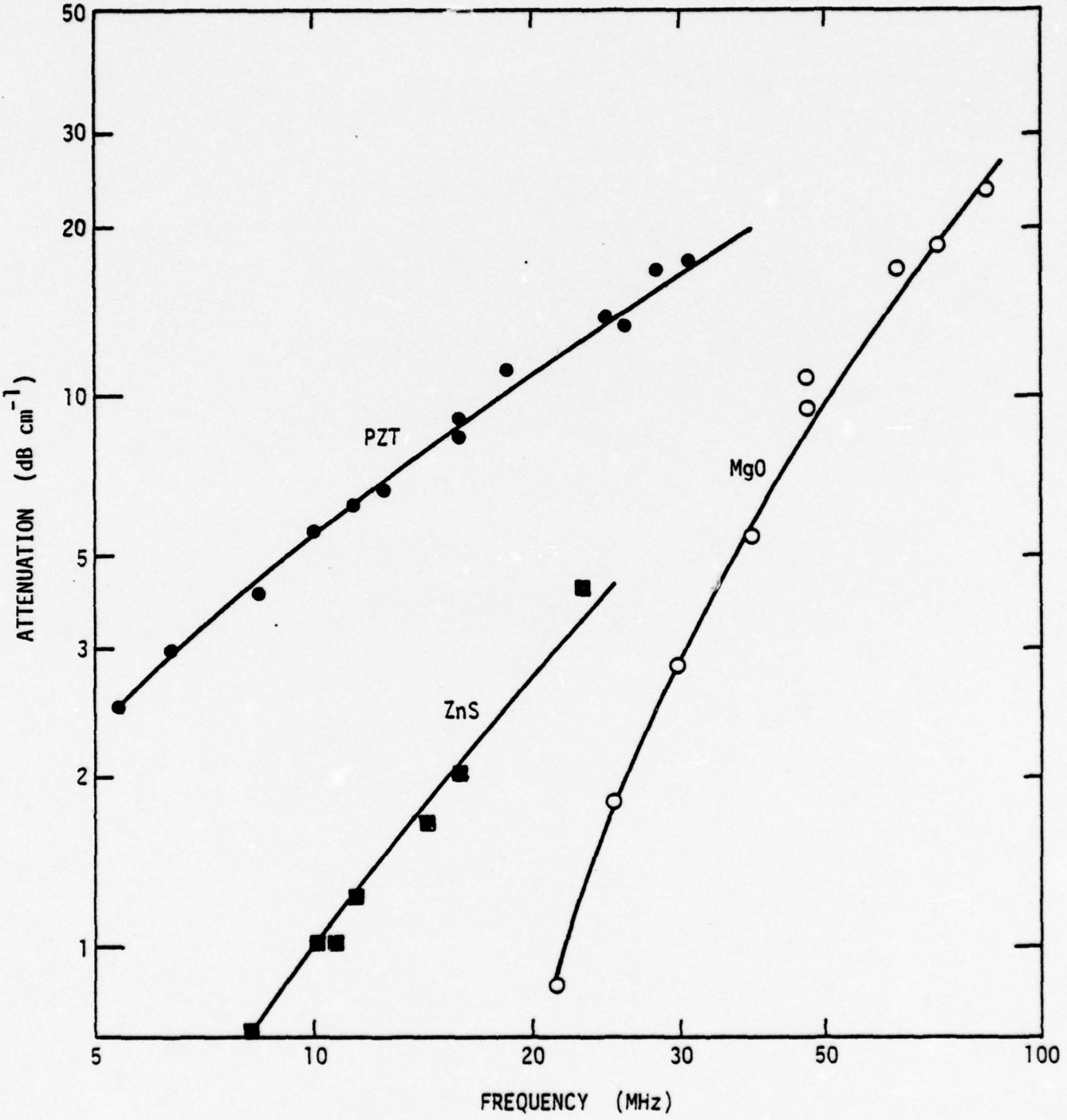
50
30
20
10
5
3
2
1
ATTENUATION (dB cm^{-1})
PZT
MgO
ZnS
5
10
20
30
50
100
FREQUENCY (MHz)

Figure 3

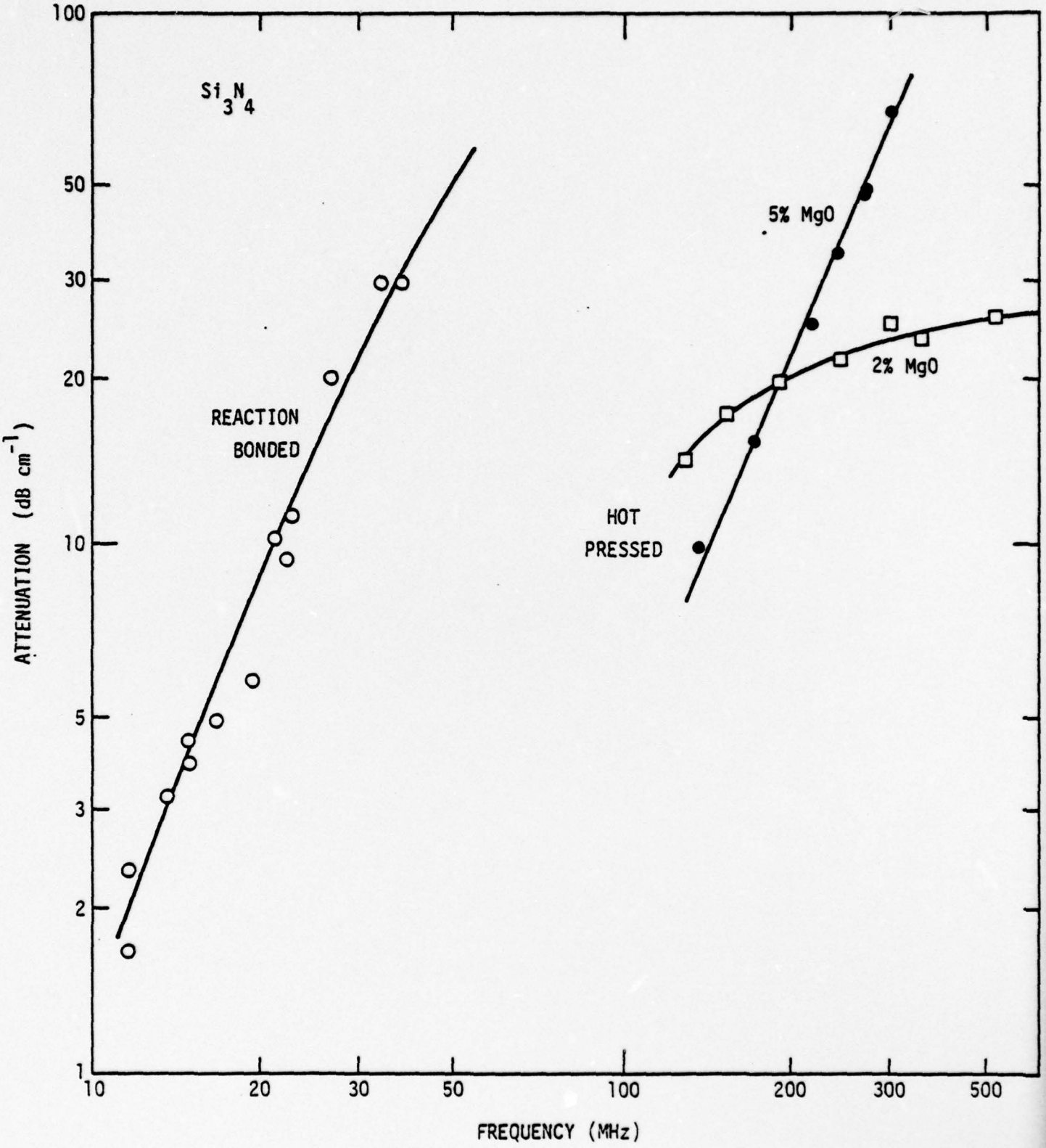
100
50
30
20
10
5
3
2
1
Si_3N_4
REACTION
BONDED
5% MgO
2% MgO
HOT
PRESSED
ATTENUATION (dB cm^{-1})
10
20
30
50
100
200
300
500
FREQUENCY (MHz)

Figure 4

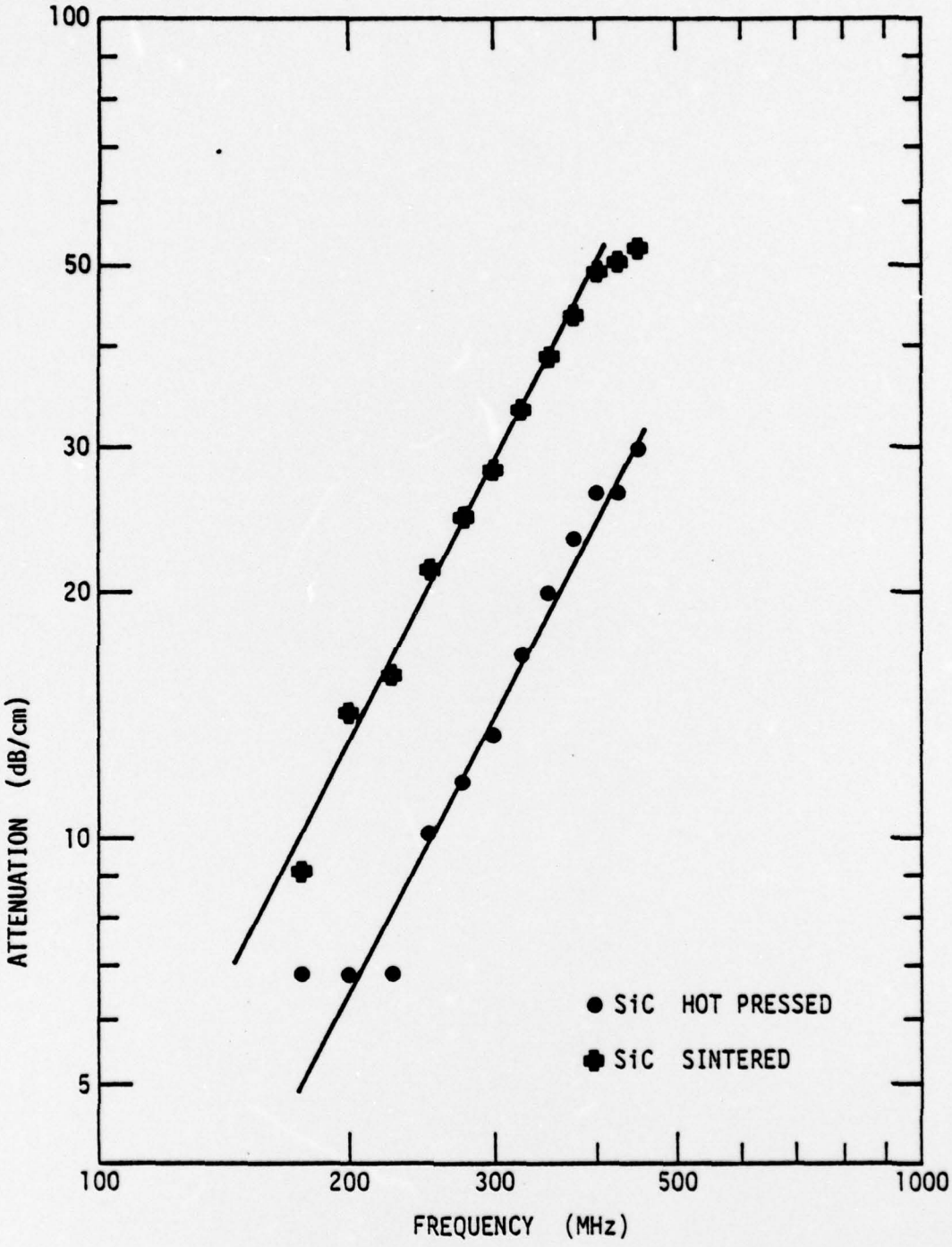
100
50
30
20
10
5
ATTENUATION (dB/cm)
100
200
300
500
1000
FREQUENCY (MHz)
SiC HOT PRESSED
SiC SINTERED

Figure 5

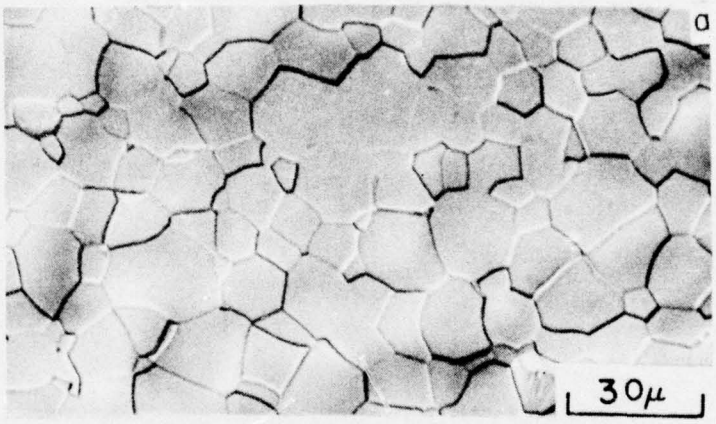

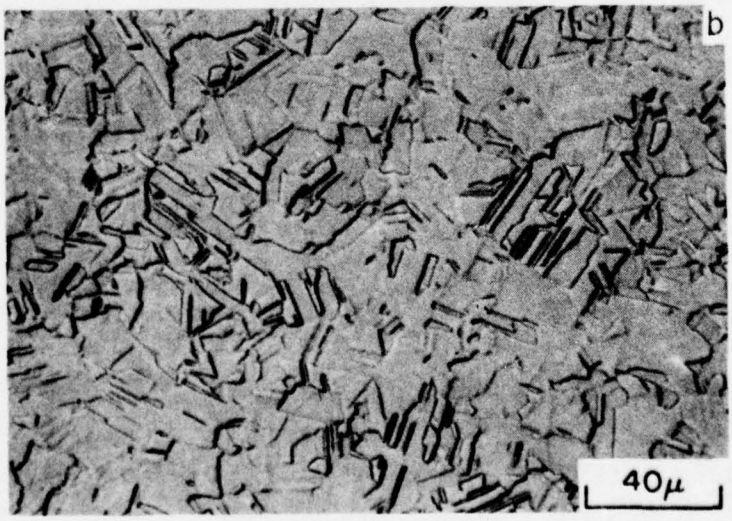

Figure 6

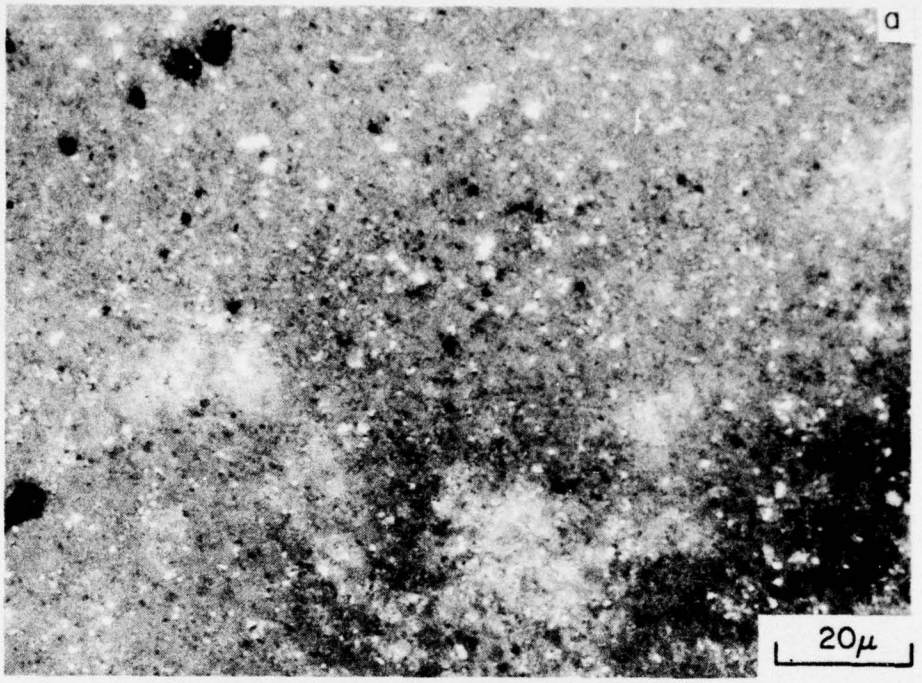

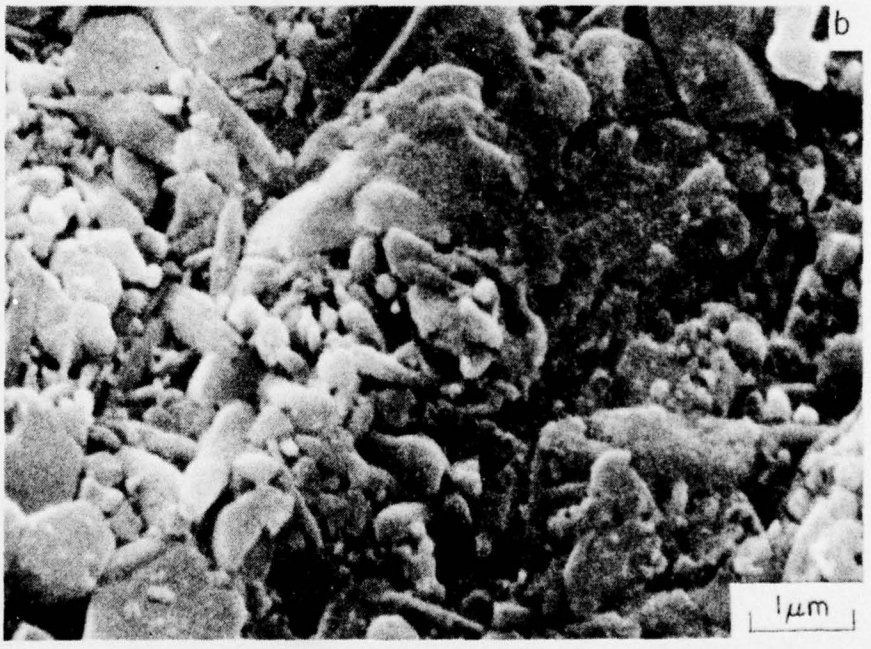

Figure 7

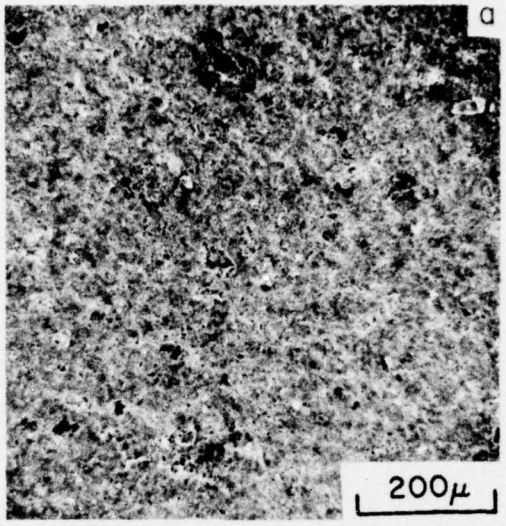

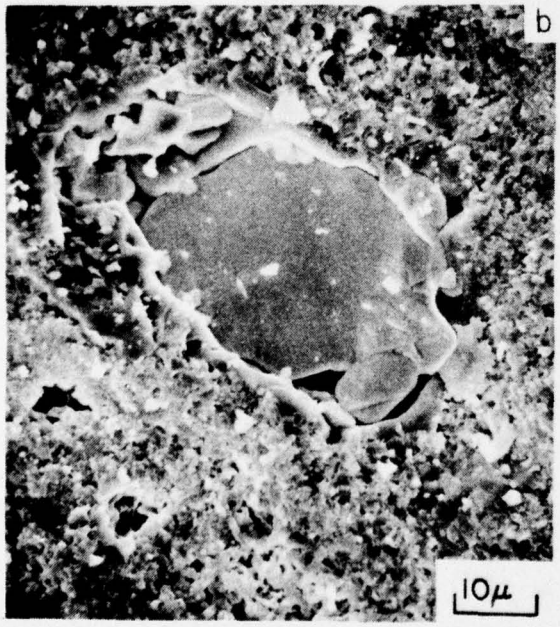

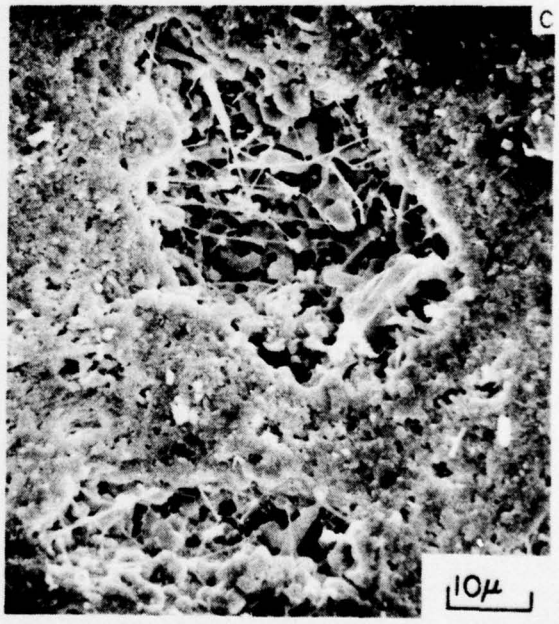

Figure 8

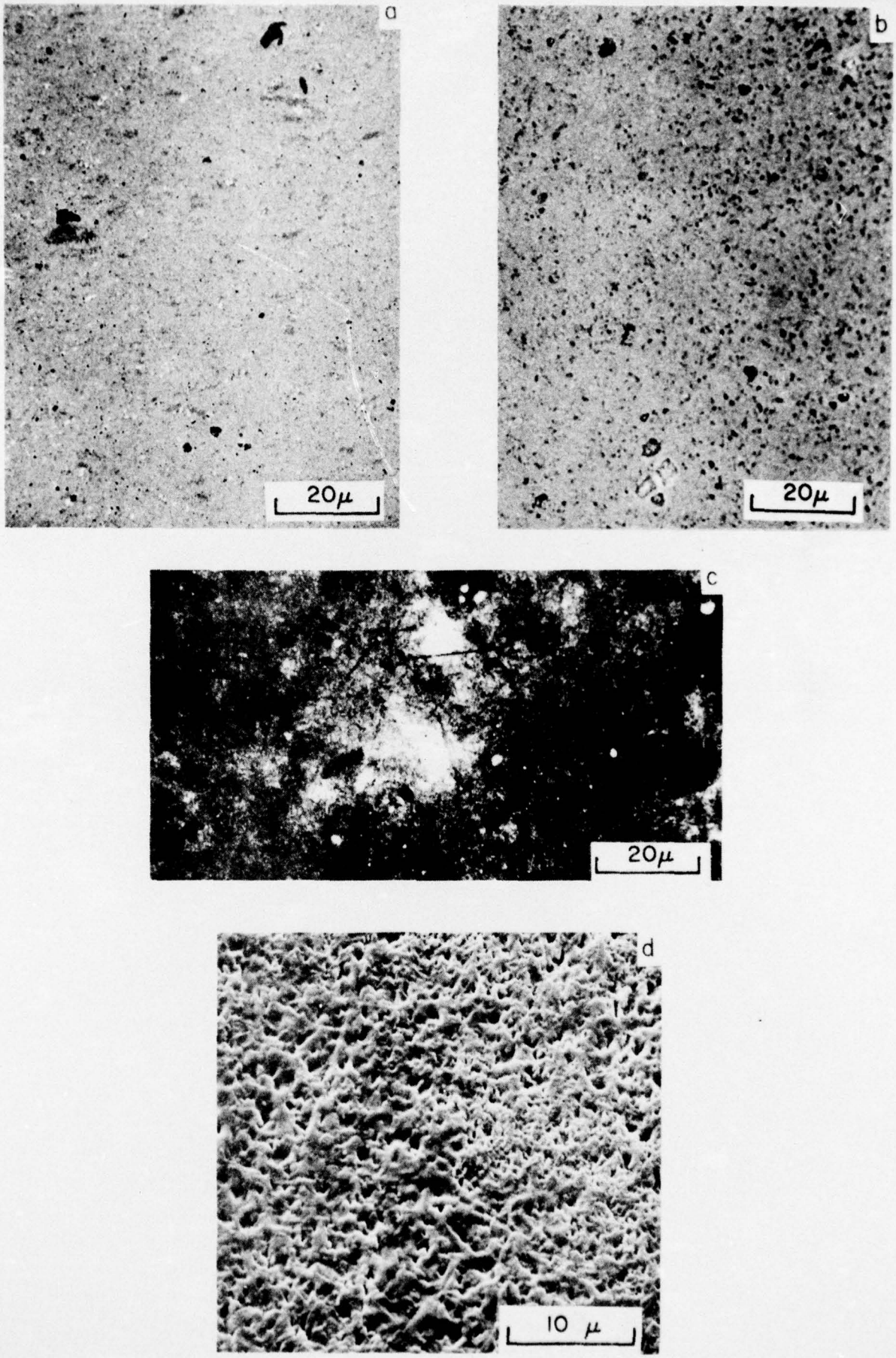

Figure 9

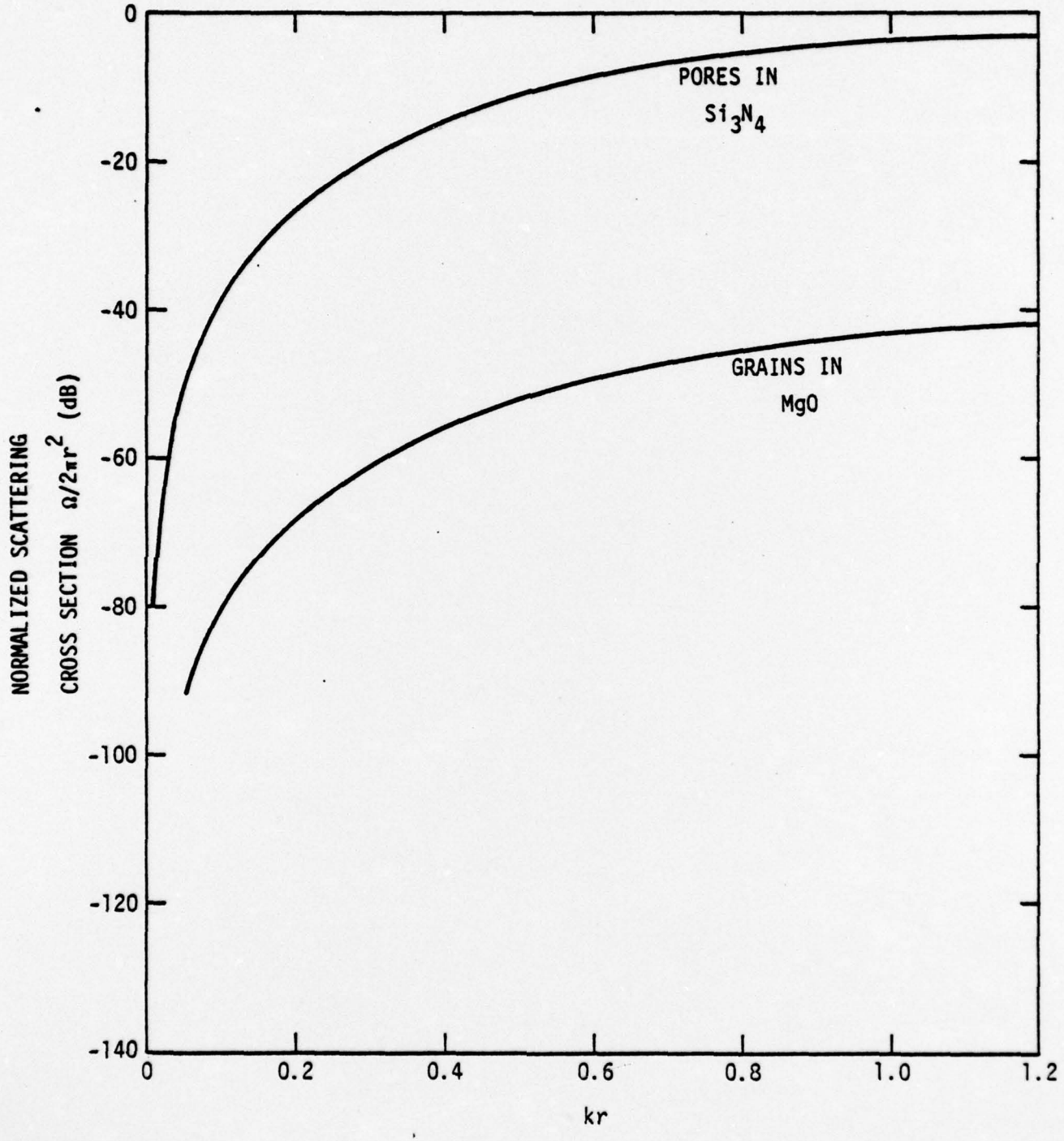
0
-20
-40
-60
-80
-100
-120
-140
0
0.2
0.4
0.6
0.8
1.0
1.2
kr
NORMALIZED SCATTERING
CROSS SECTION σ/2πr² (dB)
PORES IN
Si3N4
GRAINS IN
MgO

Figure 10

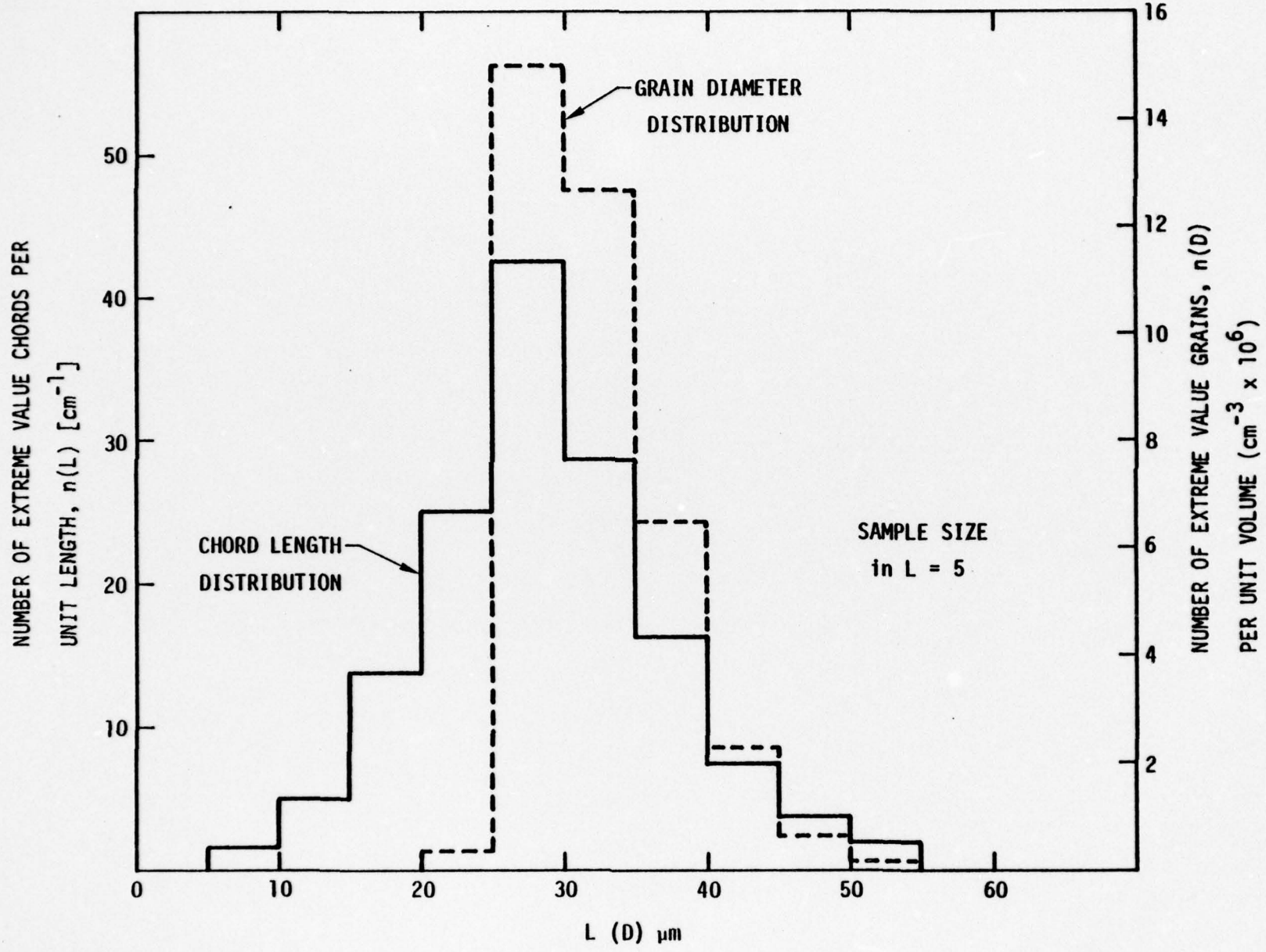
GRAIN DIAMETER
DISTRIBUTION
CHORD LENGTH
DISTRIBUTION
SAMPLE SIZE
in L = 5
NUMBER OF EXTREME VALUE CHORDS PER
UNIT LENGTH, n(L) [cm^{-1}]
NUMBER OF EXTREME VALUE GRAINS, n(D)
PER UNIT VOLUME (cm^{-3} x 10^{6})
L (D) μm
0
10
20
30
40
50
60
10
20
30
40
50
2
4
6
8
10
12
14
16

Figure 11

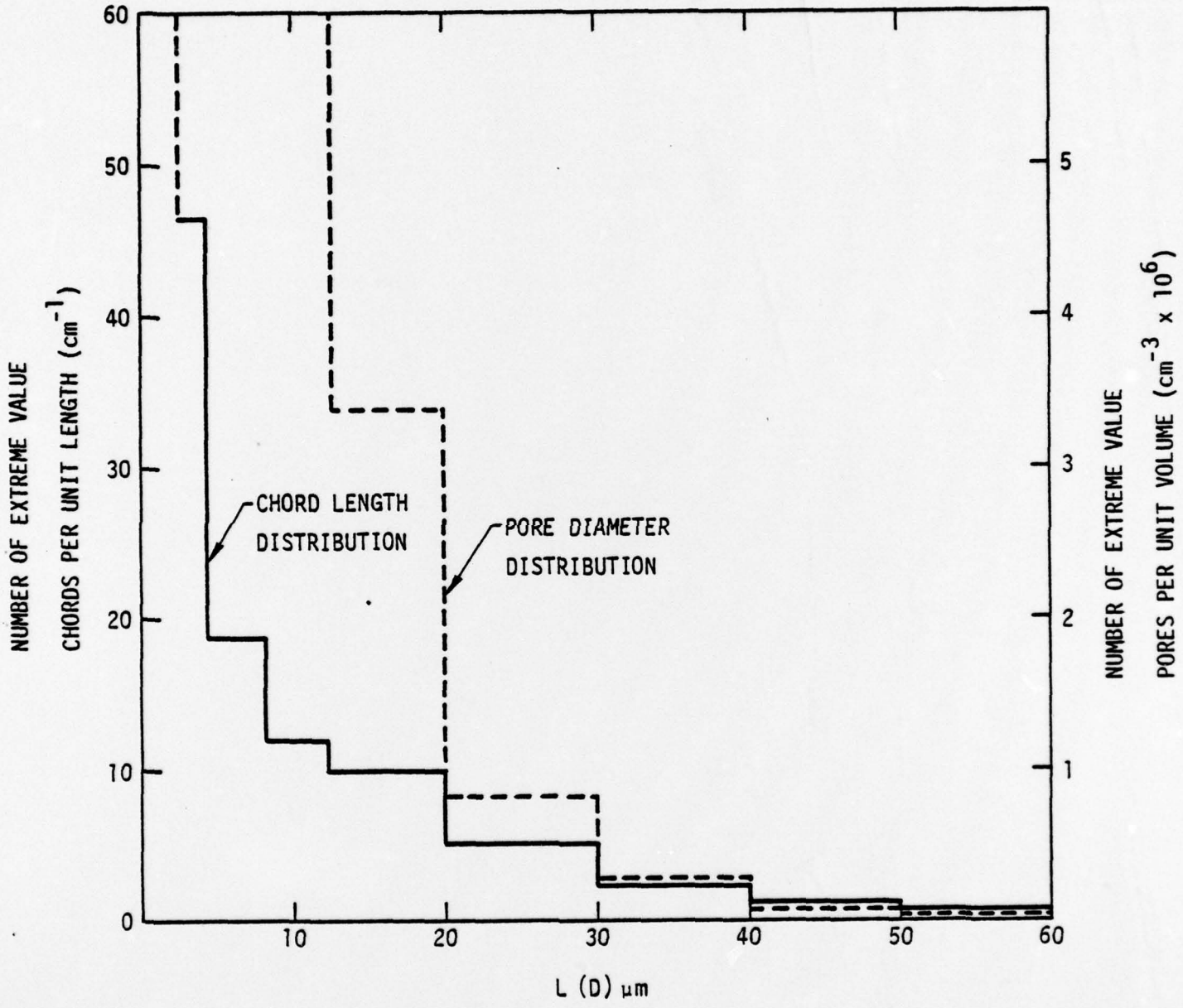
NUMBER OF EXTREME VALUE
CHORDS PER UNIT LENGTH (cm^{-1})
NUMBER OF EXTREME VALUE
PORES PER UNIT VOLUME (cm^{-3} x 10^{6})
CHORD LENGTH DISTRIBUTION
PORE DIAMETER DISTRIBUTION
L (D) µm
0
10
20
30
40
50
60
1
2
3
4
5

Figure 1 2

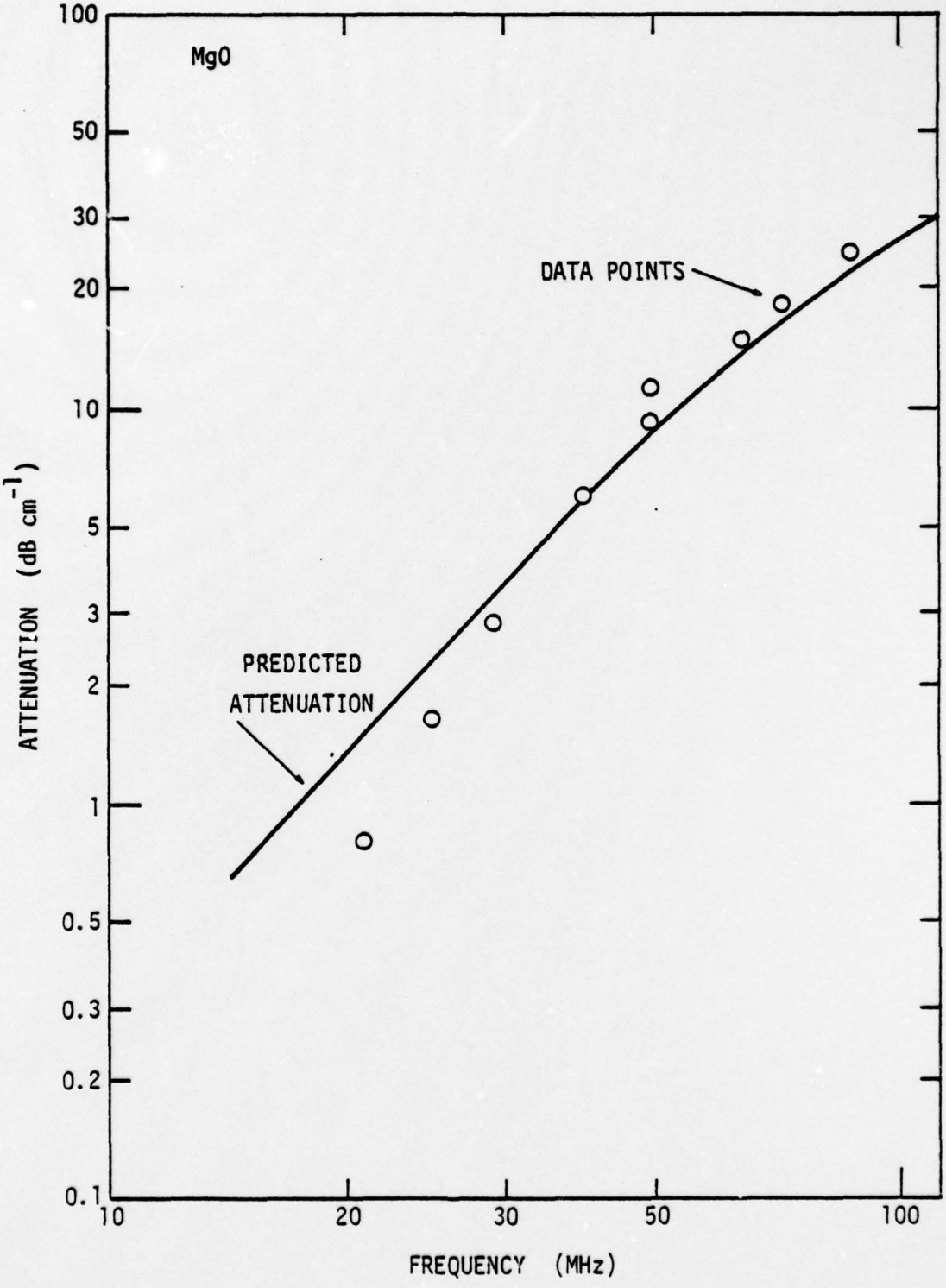
MgO
DATA POINTS
PREDICTED
ATTENUATION
ATTENUATION (dB cm^{-1})
FREQUENCY (MHz)
100
50
30
20
10
5
3
2
1
0.5
0.3
0.2
0.1
10
20
30
50
100

Figure 13 a

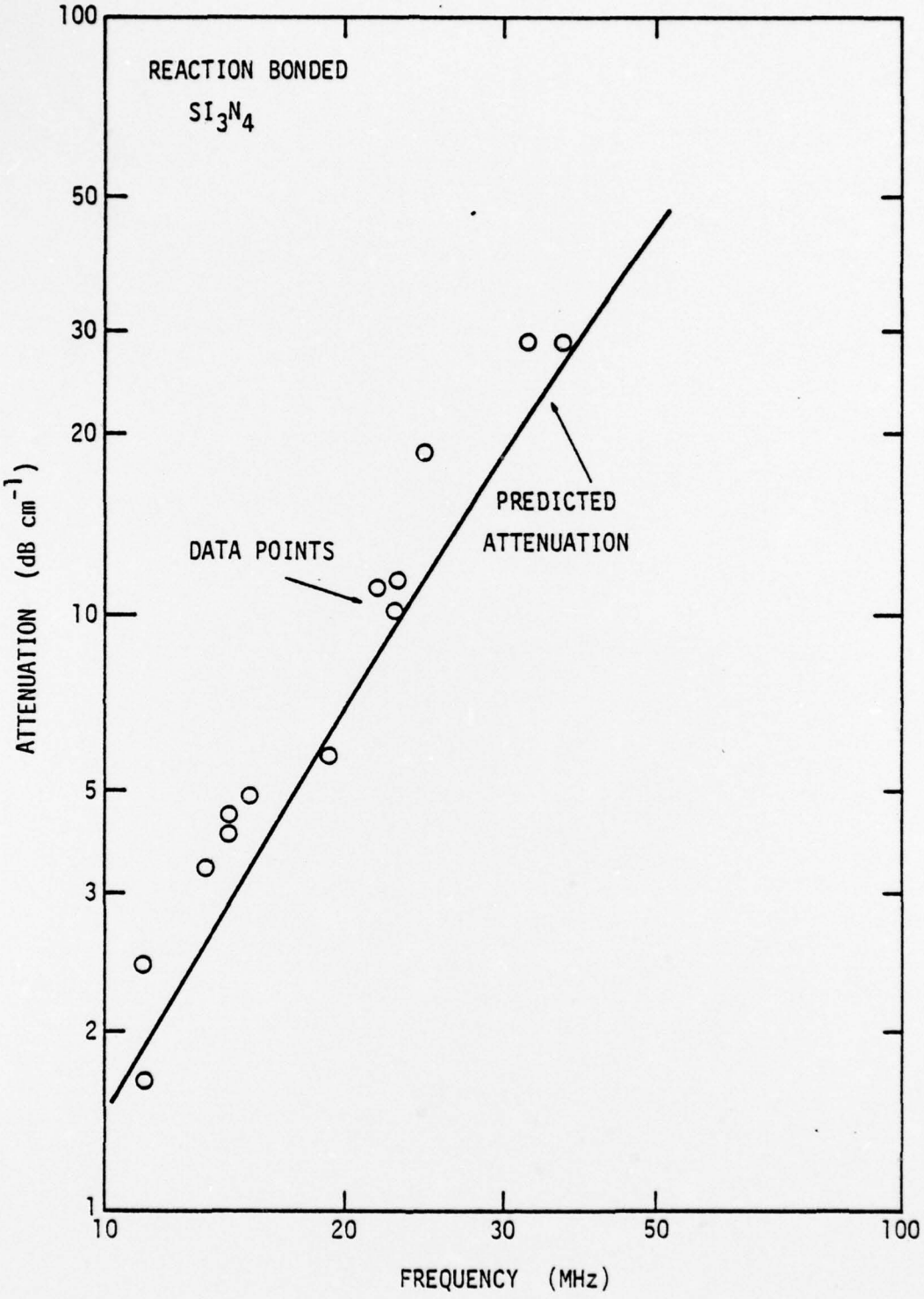
REACTION BONDED
SI_3N_4
DATA POINTS
PREDICTED
ATTENUATION
ATTENUATION (dB cm^{-1})
FREQUENCY (MHz)
100
50
30
20
10
5
3
2
1
10
20
30
50
100

Figure 13b

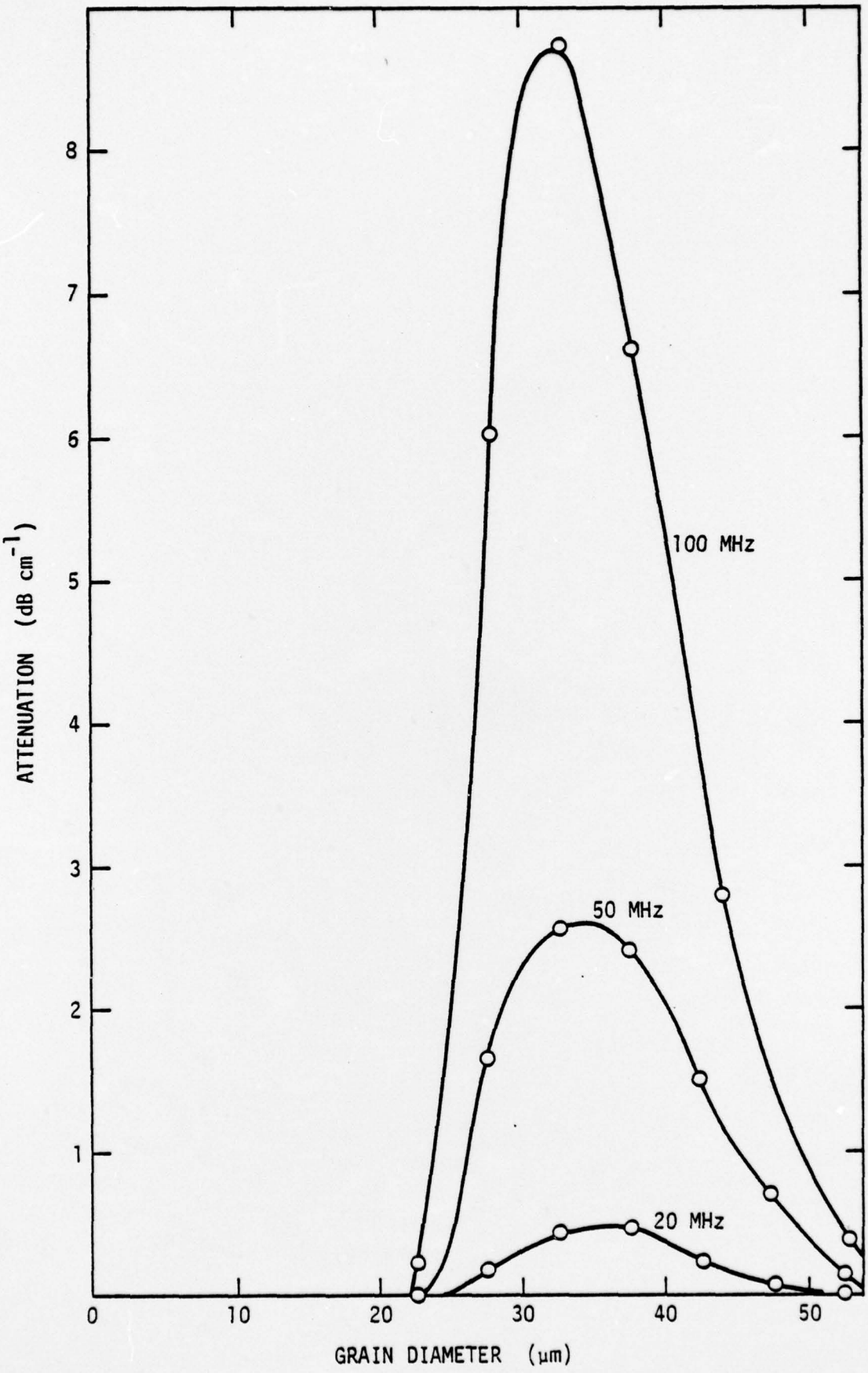
ATTENUATION (dB cm^{-1})
GRAIN DIAMETER (μm)
100 MHz
50 MHz
20 MHz
0
10
20
30
40
50
1
2
3
4
5
6
7
8

Figure 14 a

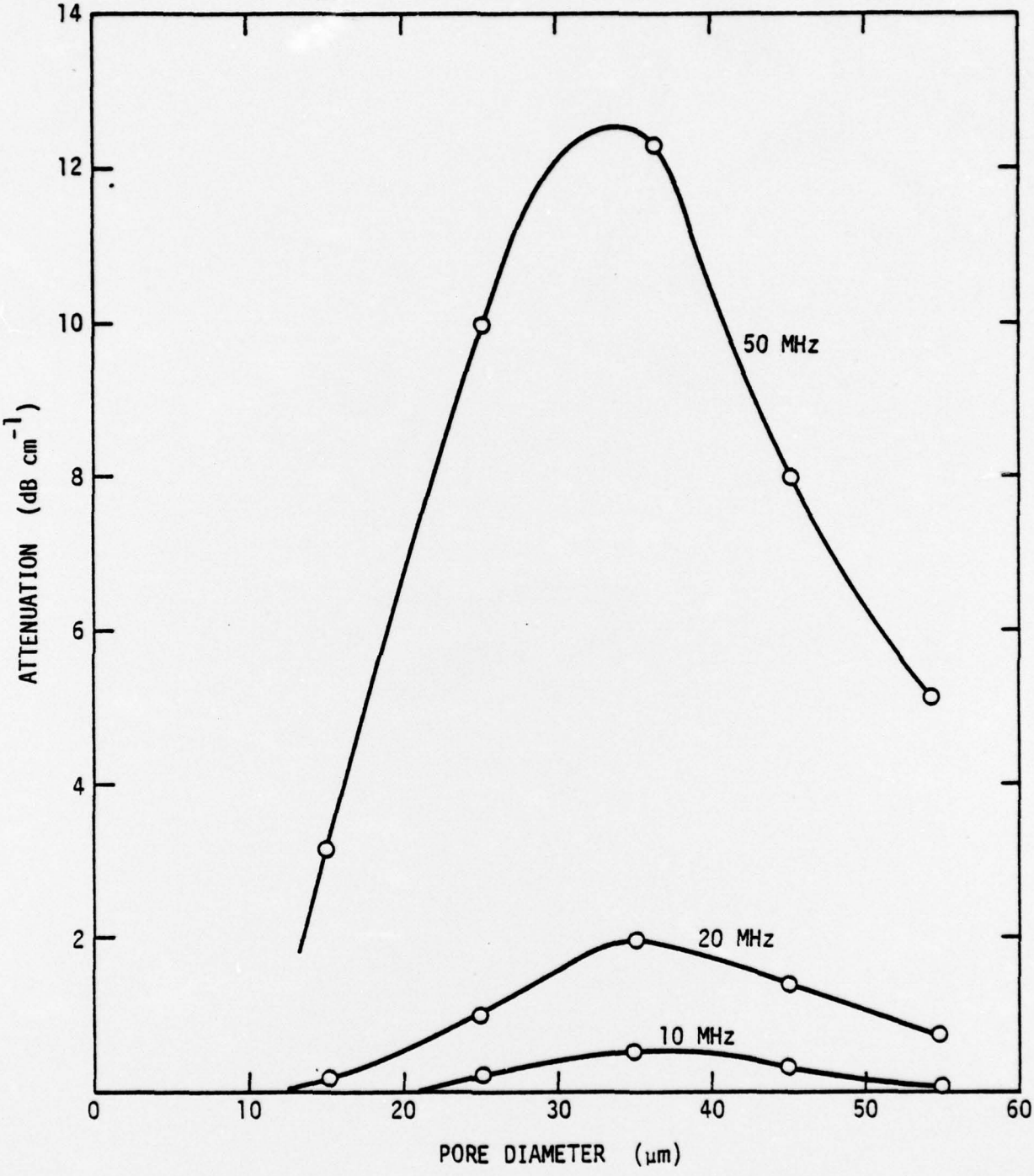
14
12
10
8
6
4
2
ATTENUATION (dB cm^{-1})
50 MHz
20 MHz
10 MHz
0
10
20
30
40
50
60
PORE DIAMETER (μm)

Figure 14 b

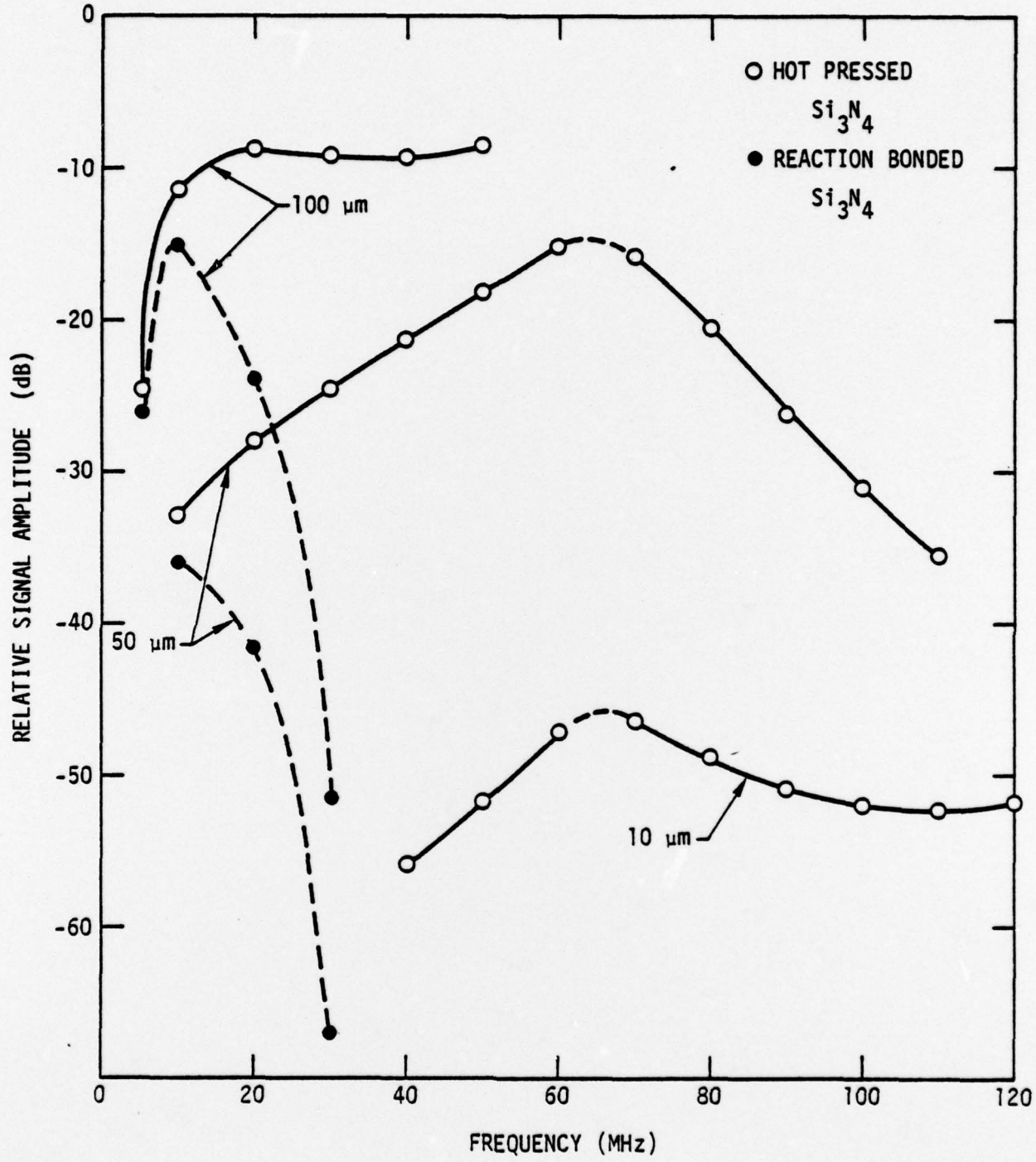
0
-10
-20
-30
-40
-50
-60
RELATIVE SIGNAL AMPLITUDE (dB)
O HOT PRESSED
Si_3N_4
● REACTION BONDED
Si_3N_4
100 µm
50 µm
10 µm
0
20
40
60
80
100
120
FREQUENCY (MHz)

Figure 15

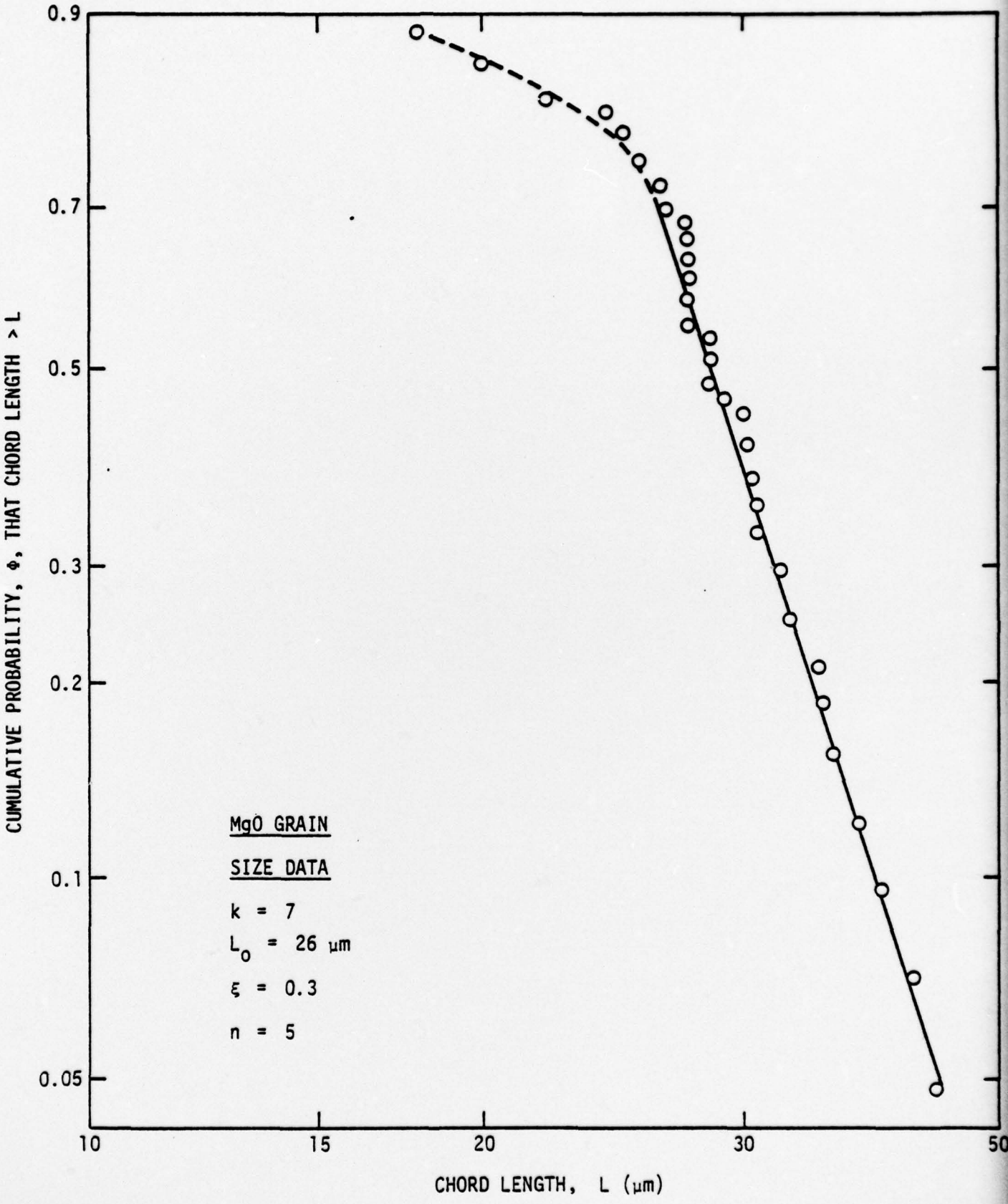
0.9
0.7
0.5
0.3
0.2
0.1
0.05
CUMULATIVE PROBABILITY, Φ, THAT CHORD LENGTH > L
MgO GRAIN
SIZE DATA
k = 7
L_o = 26 μm
ξ = 0.3
n = 5
10
15
20
30
50
CHORD LENGTH, L (μm)

Figure 16